RESEARCH REPORT

Institute of Transportation Studies | UNIVERSITY OF CALIFORNIA

Assessment of Maintenance Strategies for Bio-stabilization of Mudslides on Wildfire-affected Slopes

Ingrid Tomac, Ph.D., Assistant Professor, Structural Engineering Department, University of California, San Diego
Jonathon Chavez de Rosas, MS Student, Structural Engineering Department, University of California, San Diego

August 2022

UC San Diego

Report No.: UC-ITS-2021-48 | DOI: 10.7922/G2NZ85ZH

Technical Report Documentation Page

1. Report No. UC-ITS-2021-48	**2. Government Accession No.** N/A	**3. Recipient's Catalog No.** N/A
4. Title and Subtitle Assessment of Maintenance Strategies for Bio-stabilization of Mudslides on Wildfire-affected Slopes		**5. Report Date** August 2022 **6. Performing Organization Code** UC San Diego
7. Author(s) Ingrid Tomac, Ph.D. https://orcid.org/0000-0002-7969-9525 Jonathon Chaves de Rosas		**8. Performing Organization Report No.** N/A
9. Performing Organization Name and Address University of California, San Diego 500 Gilman Drive #0085 La Jolla, CA 92093-0085		**10. Work Unit No.** N/A **11. Contract or Grant No.** UC-ITS-2021-48
12. Sponsoring Agency Name and Address The University of California Institute of Transportation Studies www.ucits.org		**13. Type of Report and Period Covered** Final Report (September 2020 – March 2022) **14. Sponsoring Agency Code** UC ITS
15. Supplementary Notes DOI:10.7922/G2NZ85ZH		

16. Abstract

Wildfires in California have increased due to climate change, poor forests maintenance, and human factors. Post-wildfire mudflows frequently occur during rain events on burn scars due to loss of vegetation, change of surface morphology, and soil surface hydrophobicity. Spreading Xanthan gum biopolymer on slopes after wildfires may mitigate the risk of extensive erosion of hydrophobic soil layers during rain. Experiments test identified rain intensities from 15 mm/hr to 50 mm/hr and seven natural rain events on a separate set of experiments on fine, medium, and coarse sand slopes 10° to 25°. Different approaches to Xanthan gum application are considered. Surficial erosion occurs due to rain and is extreme in untreated slopes in all three sand types. Sprinkling surfaces with pure Xanthan gum leads to erosion as well. However, when xanthan gum is mixed with sand in small quantities and wetted, gel-like connections form between sand particles, which prevents further erosion when allowed to harden. Experiments focused on cured Xanthan gum and sand mix covers yielded a better understanding of coupled conditions necessary for successful erosion mitigation and the advantages and limitations of the proposed approach. Furthermore, practical guidelines for improving burned scars are recommended.

17. Key Words Wildfires, mudflows, erosion, rain, slope stability, soil stabilization, climate change, experiments		**18. Distribution Statement** No restrictions.	
19. Security Classification (of this report) Unclassified	**20. Security Classification (of this page)** Unclassified	**21. No. of Pages** 51	**22. Price** N/A

Form Dot F 1700.7 (8-72) Reproduction of completed page authorized

About the UC Institute of Transportation Studies

The University of California Institute of Transportation Studies (UC ITS) is a network of faculty, research and administrative staff, and students dedicated to advancing the state of the art in transportation engineering, planning, and policy for the people of California. Established by the Legislature in 1947, ITS has branches at UC Berkeley, UC Davis, UC Irvine, and UCLA.

Acknowledgments

This study was made possible through funding received by the University of California Institute of Transportation Studies from the State of California through the Road Repair and Accountability Act of 2017 (Senate Bill 1). The authors would like to thank the State of California for its support of university-based research, and especially for the funding received for this project.

Disclaimer

Institute of Transportation Studies | UNIVERSITY OF CALIFORNIA

Assessment of Maintenance Strategies for Bio-stabilization of Mudslides on Wildfire-affected Slopes

Ingrid Tomac, Ph.D., Assistant Professor, Structural Engineering Department, University of California, San Diego
Jonathon Chavez de Rosas, MS Student, Structural Engineering Department, University of California, San Diego

August 2022

UC San Diego

Report No.: UC-ITS-2021-48 | DOI: 10.7922/G2NZ85ZH

Table of Contents

Table of Contents

List of Tables

List of Figures

Contents

Introduction

Wildfire frequency has been increasing over the past years in California and worldwide. For example, in 2021, California (CA), US had 8,786 fires burning over 2.5 million acres, posing a threat of mudflows over burn scars following a fire (Department of Forestry and Fire Protection 2022). In addition, mudflows in California the US (Figure 1) were triggered in 2021 with rain intensities as low as 8.89 mm/hr (Department of Forestry and Fire Protection 2022). Figure 2 and Figure 3 show the current wildfire incidents and burn scars in the US. With these many burn scars and fires that will create new ones, post-wildfire slope protection is needed more than ever to stop mudflows in these areas.

Figure 1. Mudflow damage a) along River Road in Monterey County, CA following the January 26-27 storm (Image courtesy of Matthew Thomas from USGS) and b) Silverado, CA following the January 28-29 storm (Luis Sinco / Los Angeles Times)

Water-repellency, or hydrophobicity, exists in nature in a small amount in forest soils but does not affect the soil cover permeability (DeBano 1981; Doerr et al. 2000; Huffman et al. 2001). However, the hydrophobicity significantly intensifies when a wildfire vaporizes and condenses fuel burn compounds into the surrounding soil. As a result, a newly post-wildfire formed surficial hydrophobic soil layer substantially reduces the infiltration of rainwater and promotes surface erosion (DeBano and Krammes 1966; DeBano et al. 1967; Meeuwig 1971; Savage 1974; Helvey 1980; DeBano 1981; Scott and van Wyk 1990; Crockford et al. 1991; Doerr et al. 1996; Huffman et al. 2001).

In recent years, standardization attempts have been made to define fire severity (Robichaud et al., 2014). The Burned Area Emergency Response (BAER) Burned Area Reports assess soil burn severity. Robichaud et al. compiled data from BAER reports on wildfires in the western US and found the mean percentage of burn severity within the fire perimeters. Since 2000, the BAER program reclassified burn severity to reflect “soil burn severity” more closely, making the data from 2000 and on not comparable with pre-2000 data. Due to this, the

realistic distribution of soil burn severity should be thus: Unburned & Low – 51%, Moderate – 33%, High – 16%. For example, measuring soil hydrophobicity in burned areas in Colorado, USA, through both the water drop penetration test and the critical surface tension, it was found that moderate burn severity (using the exact definition as BAER).

Table 1. Proportions of land classified as unburned, low, moderate, and high burn severity within fire perimeters in the western US by decade.

Based on Burn Area Reports assessed by BAER teams (Robichaud et al. 2014)				
Decade	**Unburned (%)**	**Low (%)**	**Moderate (%)**	**High (%)**
1980-89		35	33	32
1990-99		41	30	29
2000-09		51	33	16

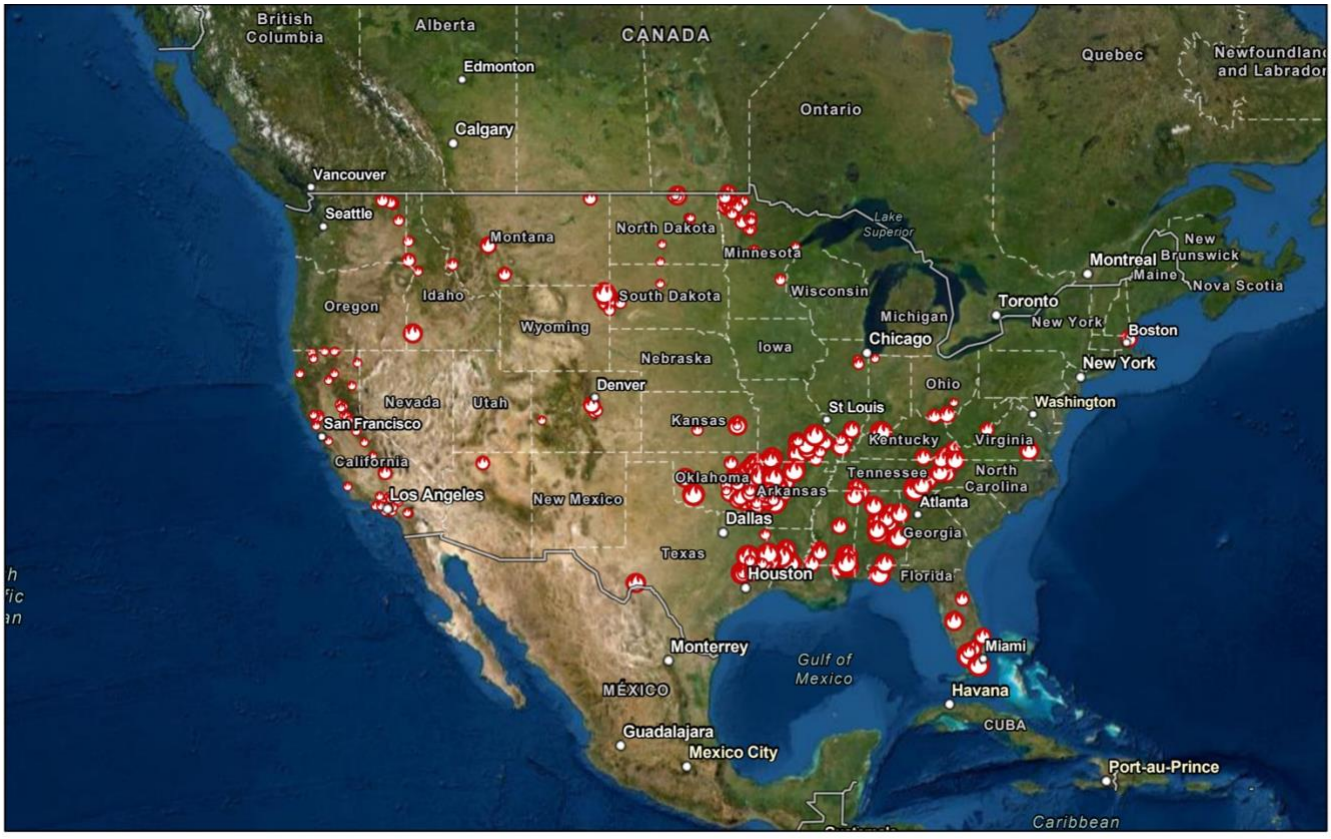

Figure 2. Wildfire incidents in the US as of March 28, 2021 (Image obtained courtesy of US Wildfire reports by Esri Disaster Response Program).

Figure 3. Burn scars in the US as of March 12, 2021 (Image obtained courtesy of US Wildfire reports by Esri Disaster Response Program)

One of the approaches to prevent erosion-triggered mudflows and debris flow on burned, hydrophobic soil is to use a temporary biopolymer cover dispersed on slopes from drones. Although previous studies showed the effects of biopolymers on improving sand shear strength and decreasing permeability, a limited number of studies use biopolymers as a post-wildfire slope mitigation technique. Furthermore, little research focused on enhancing erosion resistance by covering hydrophobic slopes with pure Xanthan gum (XG) without exploring alternative application approaches. Therefore, this research focuses on gaps in the literature regarding the effects of sand type and particle size, rain intensity, slope angle, and XG concentration, including the coupling of relevant parameters, for mitigation of post-wildfire slopes, as well as advantages and limitations of the method. Furthermore, this research investigates environmental effects by subjecting untreated and treated slopes to outside elements for six months, looking at the cumulative impacts of wind, natural rain, and animals.

XG reduces the permeability of sandy soils by filling pores (Gioia and Ciriello 2006). For example, Ayeldeen et al. (2016) determined the coefficient of permeability for sands decreased to 4% of its original untreated value at 2% XG concentration by weight after five weeks of curing. The longer the sand cures, the more permeability and hydraulic conductivity decrease, as the XG-particle links change from a gel to thinner glass-like strands (Ayeldeen et al. 2016; Cabalar et al. 2017; Moghal and Vydehi 2021). Apart from decreasing permeability, biopolymer

allows the soil to retain more water due to strong hydrogen bonding (Khachatoorian et al., 2003). In addition, the reduced permeability leads to soil plugging effects, aiding with soil remediation (Khachatoorian et al., 2003). When looking for vegetation growth improvement in drylands, just 0.5% XG implemented into the soil is enough to stimulate vegetation growth (Tran et al., 2019). The compressive strength of saturated, poorly graded Sydney sand and well-graded low-plasticity residual Piedmont soils mixed with XG increases (Lee et al., 2019; Soldo et al., 2020). For example, the 16.5% void ratio saturated soil compressive strength increases from 181 kPa to 3348 kPa, 5989 kPa, and 6185 kPa for 1%, 2%, and 4% concentration after five days of curing, respectively, with a slight decrease in strength for the 1% and 2% concentrations after 30 days (Soldo et al., 2020). Dry blending mixes and coats the surface of the particles with the biopolymer, including clays or silicate nanocomposites (Alexandre and Dubois, 2000; Akin and Likos, 2016).

XG has been used in several studies to control and mitigate wind and water erosion on slopes. For example, Kavazanjian et al. (2009) conducted wind experiments using an aluminum conduit and a fan to expose biopolymer-treated sands to approximately 26 km/hr airflow velocity. By applying an XG emulsion with a spray bottle, the soil loss percentage of experiments using 0.5% XG concentration was lowered to 0.04% from 32% observed with untreated sand. Mahayama et al. (2021) found fly ash treated with 1% XG remained undamaged, making it a suitable protective method against wind erosion, like previous work done by Chen et al. (2015), which determined mine tailings treated with biopolymers increased the penetration force. Mosavat and Tomac (2020) distributed a 4% by weight ratio of XG to base hydrophobic sand, raining over it for 100 min and collecting overflown water and eroded sand every 10 minutes. They found that the water runoff generally increased in the XG treated slopes while observing a vastly decreased soil erosion in the treated sand. Akin et al. (2021) drew the same conclusions for a slightly different setup, raining on the treated hydrophobic soil slopes sprinkled with 2.8 g of XG uniformly on a compacted soil surface for 30 min with a rain intensity of 102 mm/hr, drying, and repeating the cycle two more times. Mahayama et al. (2021) qualitatively found that fly ash and overburden mine soil were stabilized against water erosion with as little as 1% concentration of XG, with similar results found by Joga and Varaprasad (2020) for two soil types in Karnataka, India. Biopolymer increases surface erosion by reducing the erodibility coefficient from 9,132 mm/hr to 1,10 mm/hr in the specimen containing the highest sucrose concentration, stimulating the biopolymer dextran growth (Ham et al., 2018). The decrease in the erodibility coefficient is due to the shear strength increase from cohesion. Thus, a similar conclusion can be drawn for XG as Soldo et al. (2020) found the cohesion increased by 3.2 after five days of curing.

Advantages and Limitations of Xanthan Gum for Post-Wildfire Surface Erosion Control

Overview of Mudflows and Rain Intensities

Post-wildfire mudflows frequency has been increasing in the last decade. Literature review and other available public data reveal that post-wildfire mudflows are triggered by a wide range of rain intensities and rain types. Case studies of recent post-wildfire mudflows serve as a basis for determining the experimental rain intensity ranges.

A case study for the 2018 Montecito, CA debris flows found that the highest average hourly rainfall intensity that triggered the debris flow around 4:30 AM PST on January 9th of that year was slightly higher than 10 mm/hr, with an instantaneous rainfall intensity of 50 mm/hr a few minutes before the debris flow occurred (Tiwari et al. 2020). It was also found that the cumulative rainfall over the three-day storm was around 37.5 mm, which can be seen in Figure 4, courtesy of the work done by Tiwari et al (2020).

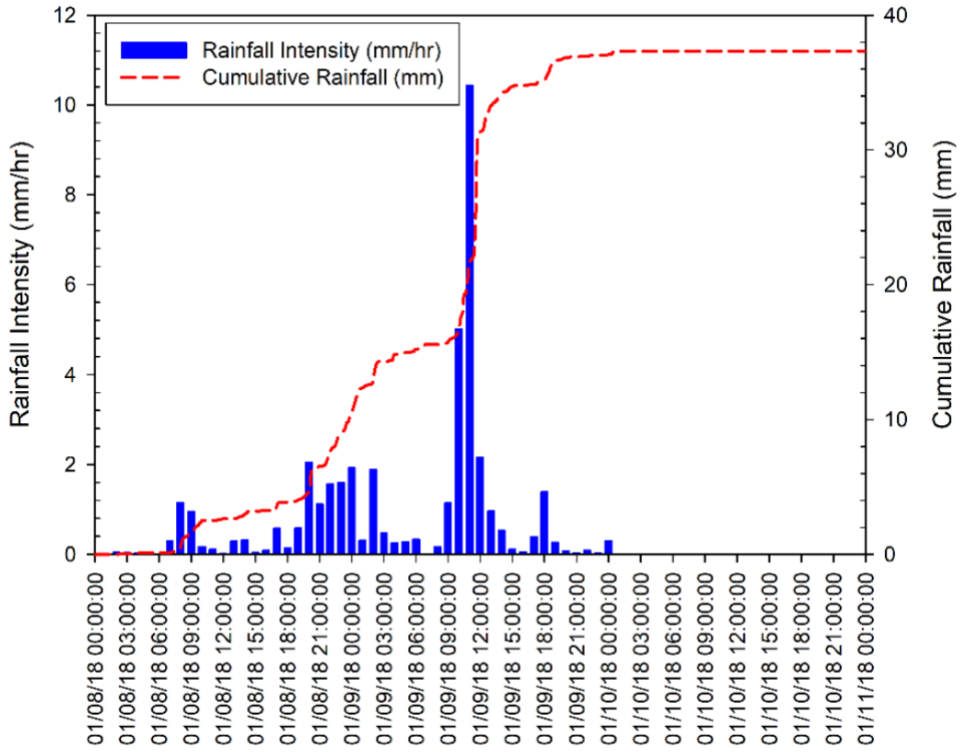

Figure 4. Time series of hourly rainfall intensity and cumulative rainfall from the January 8 to January 10 storm. All times shown are in GMT (Tiwari et al. 2020)

Oakley et al. (2017) conducted a study in which earlier work was extended for 19 precipitation events ranging from 1980 to 2014 using developed understanding of atmospheric rivers (ARs) and closed lows. ARs, defined as narrow regions of enhanced water vapor transport in the lower troposphere, can lead to increased precipitation in mountain ranges when they make landfall (Ralph et al. 2016). CLs are defined as an area of low pressure with a distinct center of cyclonic circulation that can be completely encircled by one or more height contours (Oakley et al. 201315; NOAA 201116). Within the 19 precipitation events studied, ARs were the atmospheric event for 11 out of 19, with the lowest rainfall range being 5-11 mm/hr, and 21 mm/hr when observed over 15 minutes taking place in La Cañada Flintridge, CA on December 12, 2009 within the Station burn scar. The highest average rainfall rate was 5-33 mm/hr in San Bernardino, CA on December 25, 2003 within the Grand Prix and Old fire burn scars.

While higher rainfall intensity rates were found for 15-minute intervals, the average hourly rainfall intensity rates are consistent with the average hourly rates found during this research for various post-wildfire mudflows that occurred late January of 2021. Figure 5 shows the two mudflows within California focused on to gather more rain intensity data. Through the California Nevada River Forecast Center, precipitation maps and hourly precipitation summaries for their rain station network was acquired. The text files containing the precipitation summaries were each edited to make the files readable within MATLAB. A code was created to read and extract precipitation data from the files according to the station being analyzed, and the data was then converted to metric units and plotted. Figure 5a shows the first of the two mudflows, which is a flow that occurred in Monterey County, CA along River Road in the early hours of January 27, 2021. The rain gauge station location is within the burn scar in Figure 6.

Figure 5. a) Two Southwestern U.S. burn scars focused on to gather more rain intensity data (Image obtained courtesy of US Wildfire reports by Esri Disaster Response Program) and b) River Fire burn scar in Monterey County, CA. The fire burned on August 16, 2020

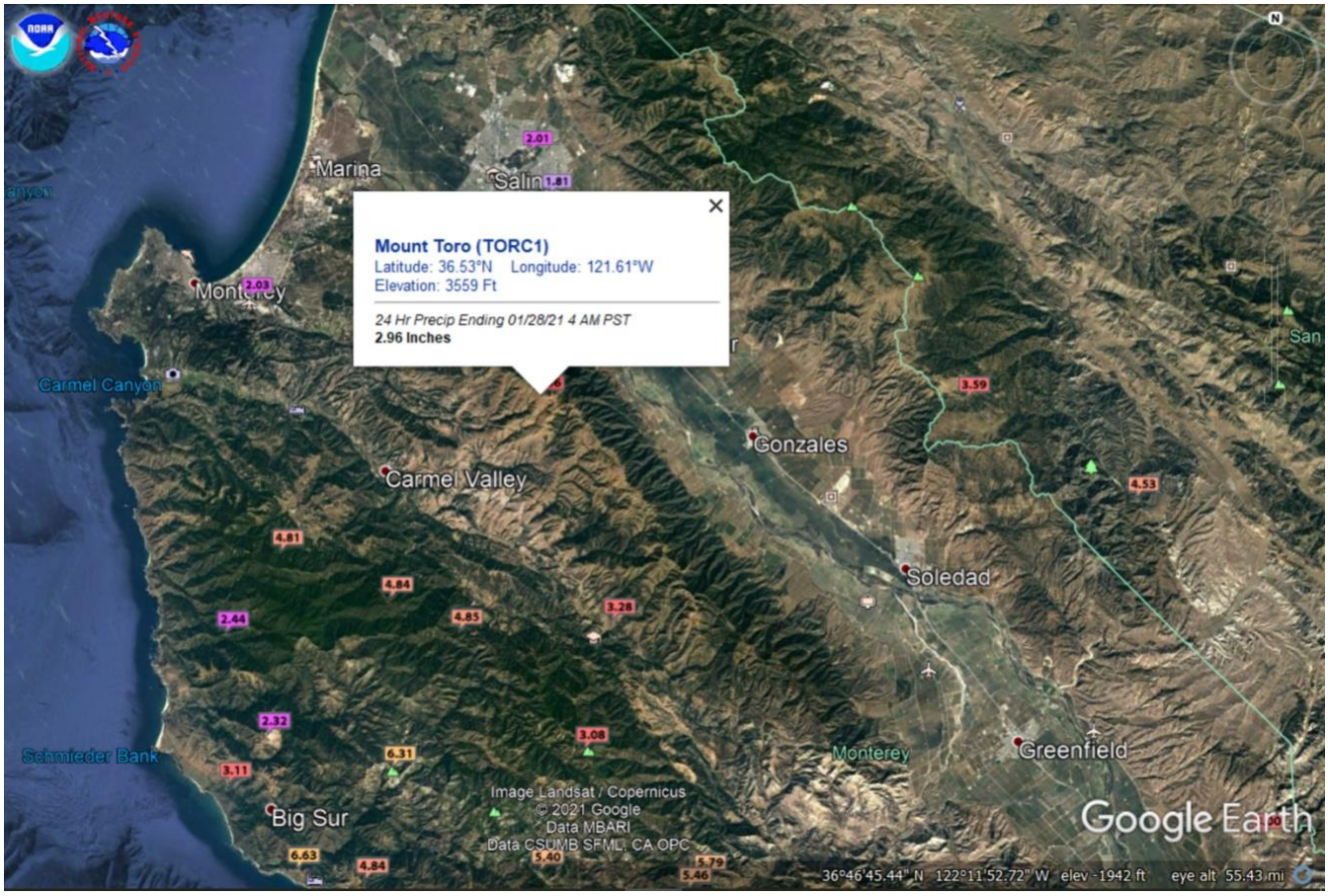

Figure 6. Rain gauge station location within the River Fire burn scar (Image obtained courtesy of NOAA)

Such as stated before, the data did not provide measurements for time periods shorter than an hour, but the hourly average rain intensities fall within the varying ranges for which post-wildfire mudflows have occurred. As seen in Figure 7, the maximum hourly rainfall intensity was 8.89 mm/hr at 4 AM PST on January 27, which was around the time the flow is thought to have started. The cumulative rainfall after it stopped raining was 23.9 mm, but as soon as it began to rain again, the total cumulative rainfall was found to be 83.1 mm although no more mudflows were reported during this time.

Figure 8 shows the second of the two mudflows, which is a flow that occurred in Silverado, CA in the last hour of January 28, 2021. The rain gauge station location is within the burn scar and can be found in Figure 9. As seen in Figure 10, the maximum hourly rainfall intensity was 12.19 mm/hr at 11 PM PST on January 27, which was around the time the flow is thought to have started. The cumulative rainfall after the storm was 39.4 mm.

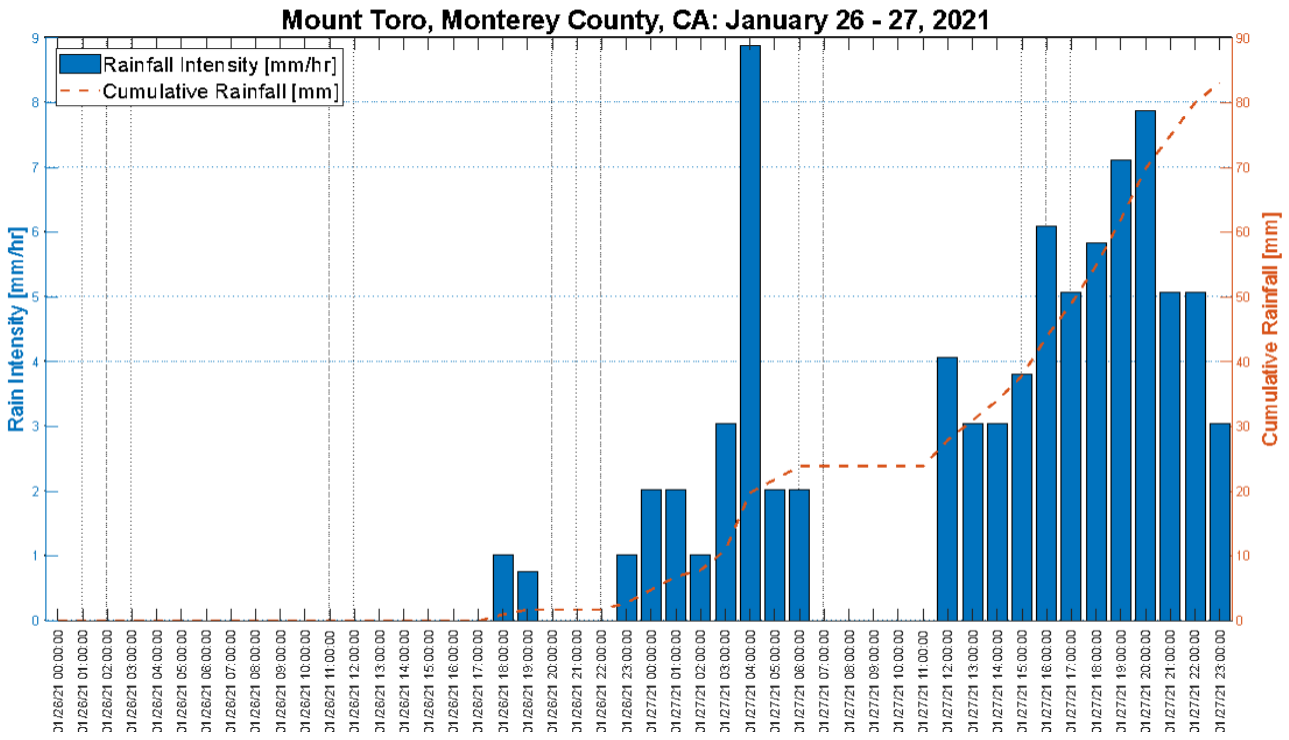

Figure 7. Time series of hourly rainfall intensity and cumulative rainfall from the January 26 to January 27 storm. All times shown in PST

Figure 8. Bond Fire burn scar in Silverado, CA. The fire burned on December 3 through December 10, 2020

Figure 9. Rain gauge station location within the Bond Fire burn scar (Image obtained courtesy of NOAA)

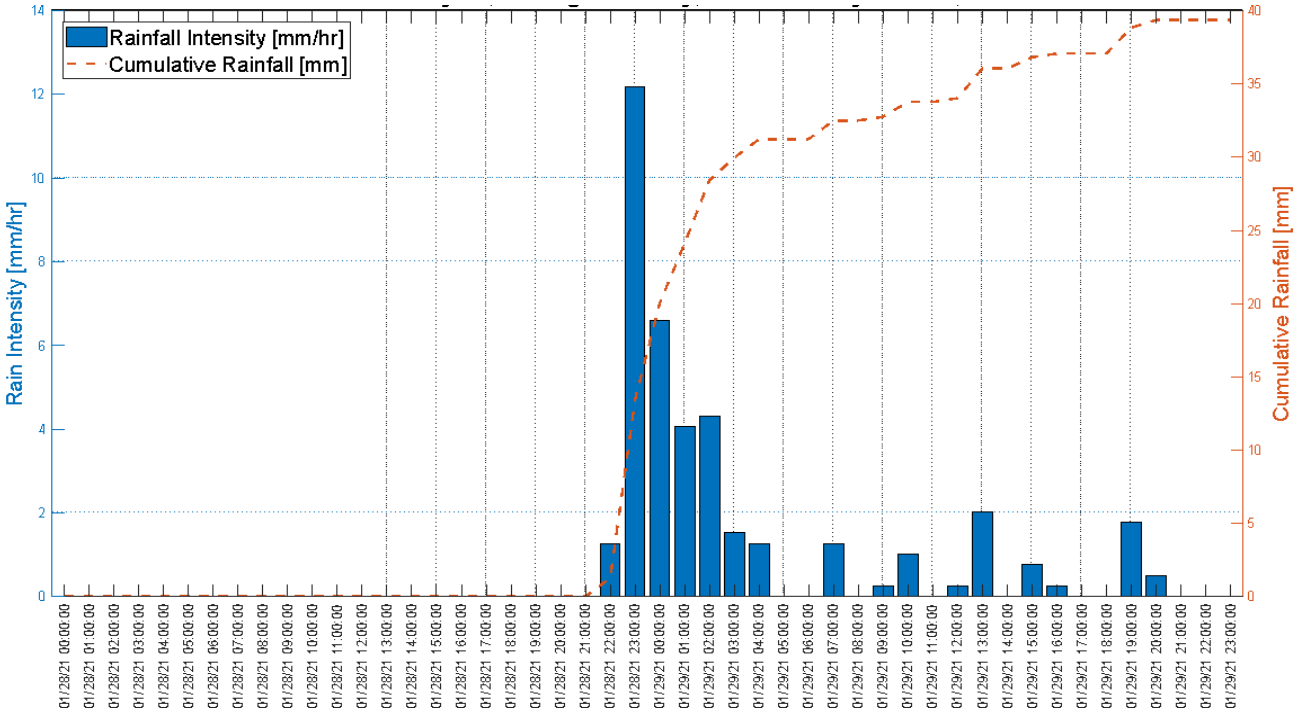

Figure 10. Time series of hourly rainfall intensity and cumulative rainfall from the January 28 to January 29 storm. All times shown in PST

Experimental Setup and Methodology

In preparation for the larger scale experiments outside, the rain system was moved outdoors. Figure 11 1 shows a 99.1 cm by 99.1 cm box made of wood and plywood with wheels for easy manipulations. The inner dimensions are 91.4 cm by 76.2 cm, with a 1.9 cm high wood plank that allows the water and superficially eroded material collection. Angled barriers guide sand and water runoff into a catchment at the bottom of the slopes. A zinc-plated slotted angles frame connected with nuts and bolts supports the experiment box and adjusts the slope.

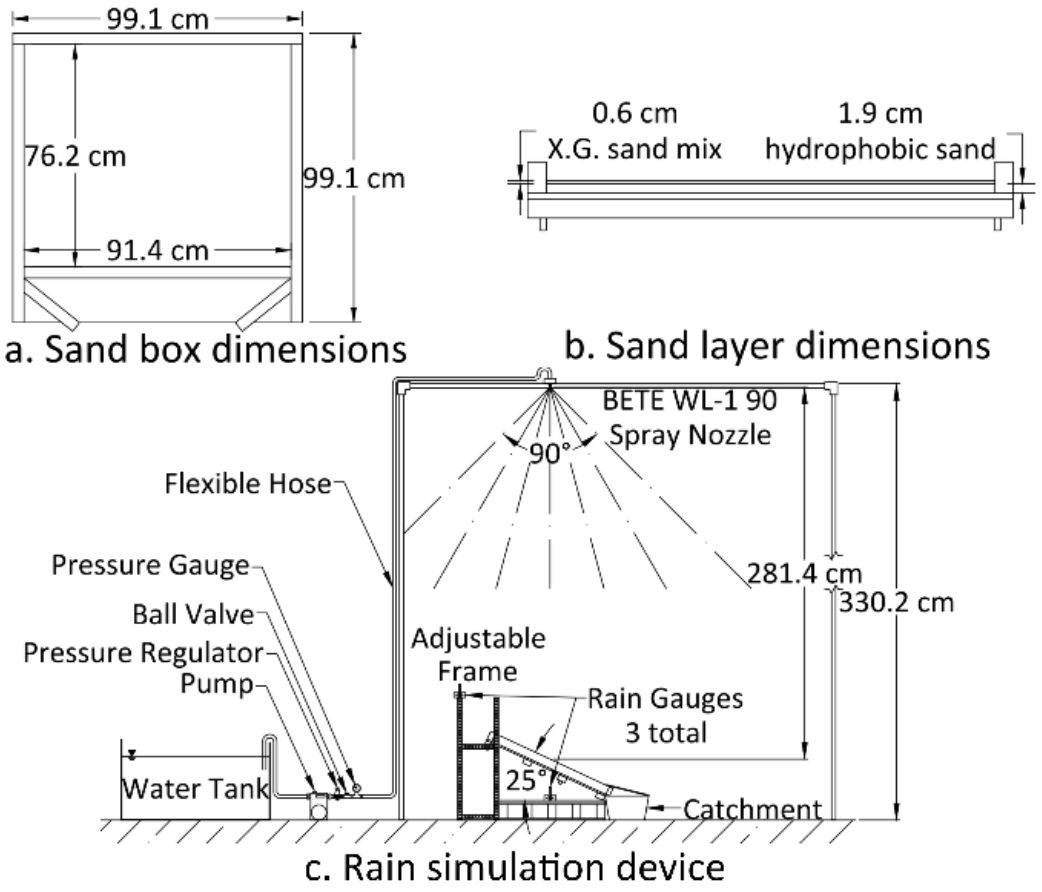

Figure 11. Outdoor rain simulation device set-up

Fine, medium and coarse sand properties are shown in Table 2 and Figure 12. Severely hydrophobic sand had already been made for use in the smaller experiments, but larger quantities are made to fill the required volume of the outdoor experiments. The water drop penetration test classifies the sand as severely hydrophobic for each batch. The preparation process follows the same procedure outlined by Movasat and Tomac (2020). The preparation process for making the hydrophobic sand is to first wash the soil until it is

clean, and the water runs clear, drying the clean soil in an oven for 48 hours. It is then submerged in a 10% noctyltriethoxysilane and 90% isopropyl-alcohol solution by volume for another 48 hours. After this, the submerged soil is then washed to remove any reactive compounds and oven-dried for 24 hours. The entire process spans 5 days, and the amount required to fill all the test beds is high, so the hydrophobic soil is prepared in batches for each set of experiments. While on level ground, the hydrophobic sand is uniformly distributed into the sandbox up to a height of 1.9 cm. Different setups investigate an optimal erosion control: (1) control setups with untreated hydrophobic sand, (2) setups with XG and sand mix pluviated over the hydrophobic layer, (3) 24 h cured XG-sand mix that is sprayed with 16.5% concerning the layer's mass, or 371.25 g, of water. Then, the adjustable frame is set at the target angle's height, and the sandbox is rolled over carefully and gently placed at the angle.

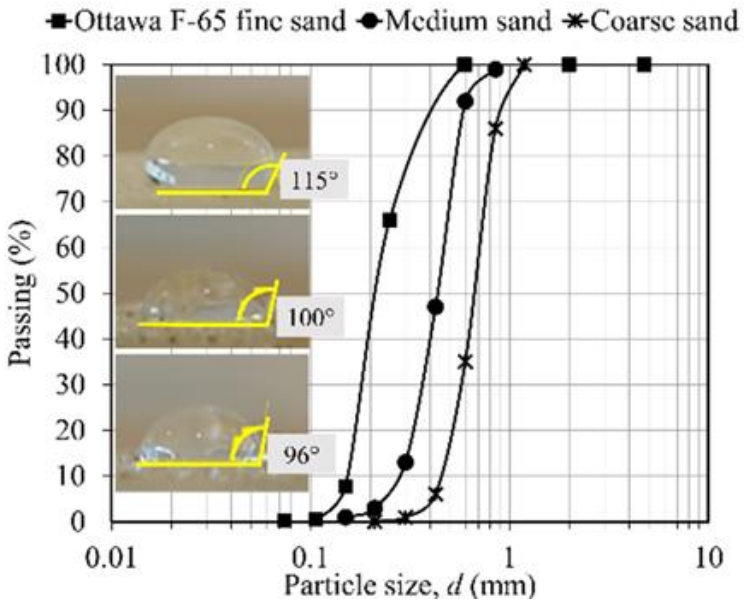

Figure 12. Granulometry of fine, medium and coarse sand, with the measured contact angles after hydrophobized

Table 2. Soil contact angle and particle grading parameters

Soil	Contact angle, q_a(°)		C_u	C_c	D_{10} (mm)	D_{50} (mm)	D_{60} (mm)	Roughness, r(Sq) (μm)
	Hydrophilic	Hydrophobic						
Fine	60	115	1.50	0.90	0.15	0.2	0.23	54.7
Medium	38	100	1.67	1.01	0.28	0.4	0.47	155
Coarse	27	96	1.53	1.03	0.46	0.65	0.70	250

Effects of Sand Type, Xanthan Gum Percentage and Slope on Erosion and Water Overflow

First, 50 mm/hr rain intensity experiments without any XG provide the erosion baseline at 10°, 15°, 20°, and 25° slopes for medium sand and 10°, 25°, and 30° for fine sand. Second, raining experiments are performed on sand slopes sprinkled with uncured XG-sand mix. Although the XG sprinkling method seemed to aid in erosion resistance at first, the surface layer soon becomes over-wetted during the trial 15 min of rain, and the whole swollen XG layer excessively deform and fails. Therefore, covering the sand surfaces with an uncured XG-sand layer increases the risk of failure for prolonged rain events. Third, sprinkling pure XG was initially considered, but indoor, small-scale experiments, with an identical rain simulation device from Tiwari Tiwari Tiwari et al. (2014) resulted in the XG-sand mix experiencing less surface morphology than the pure XG trial with multiple crater-like ridges from the raindrop impacts. Fourth, a 0.6 cm of XG mixed with hydrophilic sand layer is placed over hydrophobic sand and wetted. After drying, the XG treated soil layers solidify, like the study conducted by Soldo et al. (2020). Microscopic images of pieces of naturally re-dried crusts (Figure 13) with no deformation from each sand type show different styles of XG bonding in each sand. Figure 13 shows that in the coarse sand, XG bonds are web-like, with very tiny particles attached to them as the strands span from a large particle to another. The bonds encapsulate the particles completely in the fine sand, almost sheet-like, as seen in Figure 13c. The medium sand crust bonds seem to be a combination of the other two-crust bonds, with pure XG strands spanning from particle to particle, with an addition of inter-particle close contact cementing bonds.

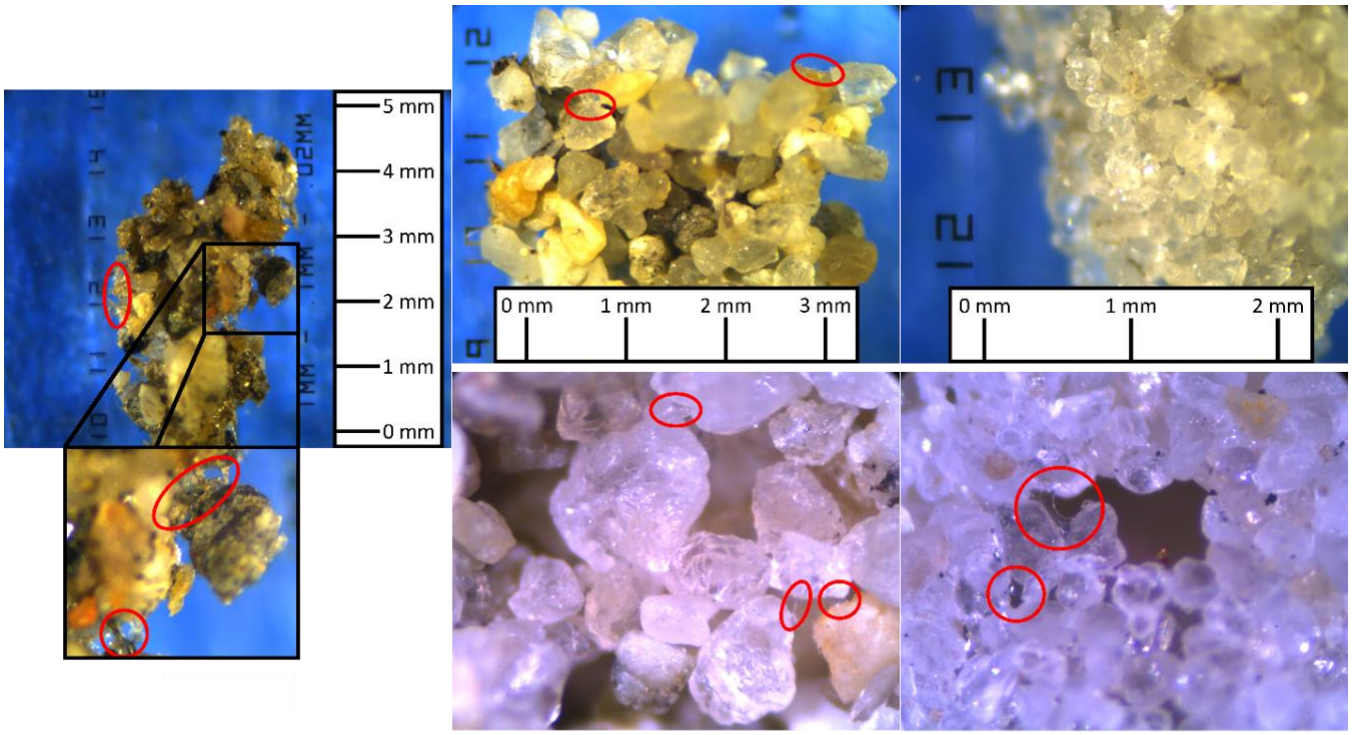

a. Coarse

b. Medium. *Top*: For scale
Bottom: For better bond view

c. Fine. *Top*: For scale
Bottom: For better bond view

Figure 13. 3% X.G. crust bonds in the three sand types

Surface Morphology

Overall, experiments reveal full and partial surficial erosion at different rain intensities, slopes, and sand types, with most treated surfaces successfully reducing erosion (Figure 14). Furthermore, several experiments treated with XG gradually develop non-favorable surface morphologies that enhance erosion or water overflow. Figure 15 classifies surface erosion morphology into six different types. Table 3 and Table 4 summarize experimental results and erosion types, including those without visible surficial changes. For example, Figure 15a shows rain erosion of untreated hydrophobic medium sand at a 15° slope. The sand surface slowly erodes under the raindrop's impact, and the erosion subsequently increases. Similar morphology evolves at the 10° and 15° medium, and 10° for fine sand slopes under higher rain intensity. Finally, preferential surficial flow channels lead to significant erosion at steep 20° and 25° untreated slopes (Figure 15b).

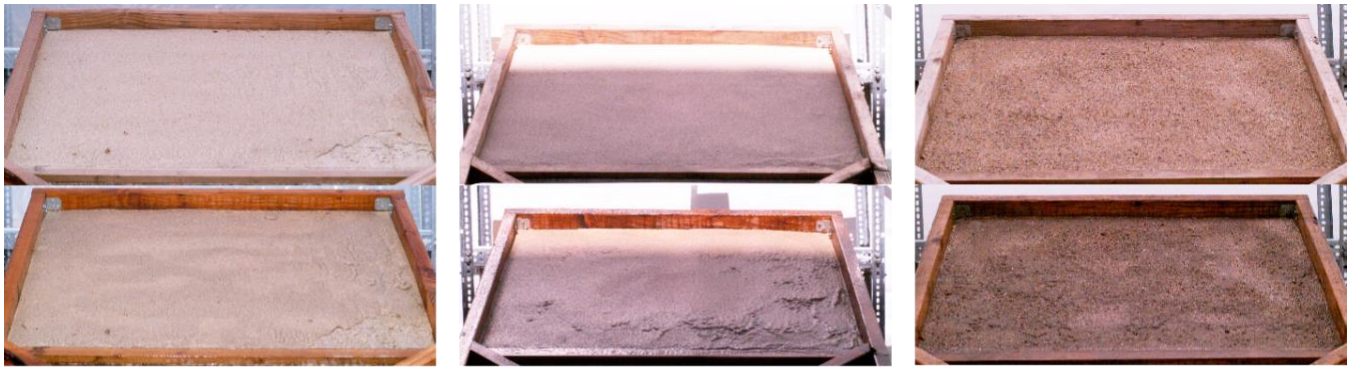

a. Medium 3% XG not cured, one day after first raining experiment. *Top*: Before *Bottom*: After

b. Medium 1% XG cured. *Top*: Before *Bottom*: After

c. Coarse 2% XG cured. *Top*: Before *Bottom*: After

Figure 14. Examples of successful experiments at 50 mm/hr rain intensities and 25°, before and after

Slopes treated with XG show either stability or minor erosion than untreated or develop surface plastic deformation. Two instances of an extreme surface morphology occur in an uncured mix of 0.5% XG and medium sand at the 20° and 25° angles, seen in Figure 15c. First, large horizontal sections slide down as the uncured mix had no solidified bonds while containing little XG. Subsequently, the exposed hydrophobic sand develops channels like the untreated slopes at these same angles. By increasing the concentration of XG in the mix with medium sand, for example, to 3%, the horizontal erosion effect persists, but at a significantly smaller scale without channels (Figure 15d). Figure 15e shows sliding ridges observed with various XG percentages in the sand and sprinkled with water cured for 24 hours. The curing process produces a crust with solid bonds between the particles (Figure 13) and less erosion. As a result, small ridges form under raindrops impact in different surface sections that then attempt to slide down while the rest of the crust holds in place. While cured, coarse sand slopes with a mix of 2% and 3% XG at 25°, medium sand experiments with 1% XG at 25° and 3% XG at 15° and 20°, and fine sand slopes with 3% XG at 20° and 25° all experienced the morphology type in Figure 15e. Figure 15f shows a morphology characterized by individual sliding patches formed when the bonds from the cured XG were not strong enough to hold the sliding sections in place. For example, individual sliding patches occur in the medium sand with a mix of 3% XG at the 20° to 25° slopes and fine sand with 1 and 2% XG at a 25° slope, while 3% XG prevents sliding patches of fine sand. In addition, while the not cured mix of 3% XG develops horizontal erosion when allowed to cure by re-drying and to test again the day after, a tiny sliding section develops.

In addition, Table 4 summarizes observations of surface morphology at a lower rain intensity of 15 mm/hr, which overall show more favorable results. Coarse and fine sands with different cured XG percentage mixes formed small ridges after 15 minutes, with little to no changes after another 15 minutes. For cured medium sand, both 1% and 3% develop very few ridges after 15 min, but after another 15 min, another surface erosion type occurs, where a small patch begins to slide down the slope for the mix of 1% XG. Furthermore, at this lower rain intensity, an uncured blend of 0.5% XG does not develop the extreme horizontal erosion and channels, but only the horizontal erosion at the smaller scale, much like the uncured 3% XG at the higher intensity.

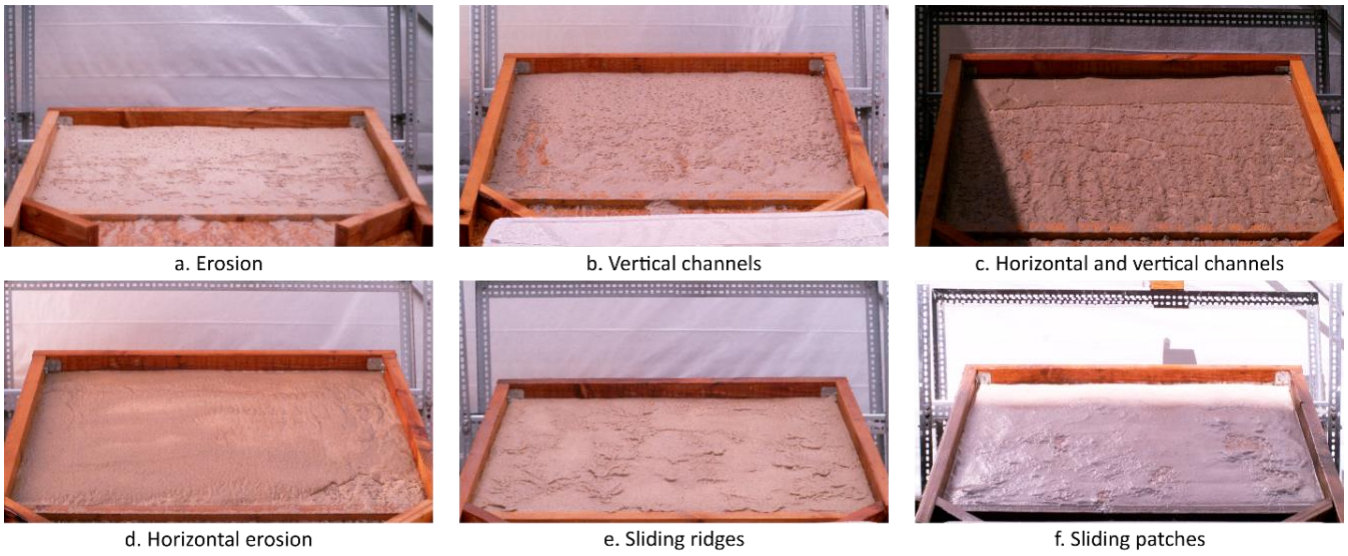

Figure 15. Observed erosion types

Table 3. Surface erosion type and runoff for each experiment with rain intensities of 50 mm/hr for 15 min

Tests	XG %	Test Type	Surface Erosion Type	Normalized Runoff		% Eroded
				Water (mL/cm2)	Soil (mg/cm2)	
10°						
Fine	0	N	Figure 15a	1.14	46.05	2.52
	3	C	None[a]	1.62	0	0
Medium	0	N	Figure 15a	1.06	37.31	2.42
15°						
Medium	0	N	Figure 15a[c]	0.16	78.45	4.68
	3	C	Figure 15e[a]	1.15	0.3	0.01
20°						
Fine	3	C	Figure 15e[a]	0.02	0.0004	0.02
Medium	0	N	Figure 15b	0.26	73.31	3.84
	1	N	Figure 15c	0.73	376.33	14.79
	3	C	Figure 15e[a,c]	1.15	0.32	0.01
Coarse	3	C	None[a]	0.23	0.64	0.02
25°						
Fine	0	N	Figure 15b	0.69	325.26	16.59
	1	C	Figure 15f[a,c]	0.62	1.327	0.05
	2	C	Figure 15f[a]	0.74	229.93	8.86
	3	C	Figure 15e[a]	0.1	0.95	0.03
Medium	0	N	Figure 15b[c]	0.59	57.96	3.46
	3	N	Figure 15d[a,c]	0.35	69.99	2.1
	3	ND	Figure 15f[a,b]	0.64	1.58	0.05
	1	C	Figure 15e[a,b]	0.4	0	0
	3	C	Figure 15f[a]	0.23	1.27	0.04
Coarse	2	C	Figure 15[a,b]	0.26	0.12	0.01
	3	C	Figure 15e[a]	0.26	0	0
30°						
Fine	0	N	Figure 15b	0.6	1446.08	65.83
Medium	1	N	Figure 15c[c]	0.79	531.97	21.82

Note: N = not cured; ND = one day after corresponding N test; C = 24h cured; [a]Successful in reducing erosion compared to untreated hydrophobic slopes; [b]Shown in Figure 15; [c]Used as reference picture in Figure 15

Table 4. Surface erosion type and runoff data for each cured experiment with rain intensities of 15 mm/hr

Tests	XG %	Rain Duration (min)	Surface Erosion Type	Normalized Runoff		% Eroded
				Water (mL/cm²)	Soil (mg/cm²)	
25°						
Fine	1	15	Figure 15e	0.02	0	0
	1	30	Figure 15e	0.07	0	0
	3	15	Figure 15e	0.24	0	0
	3	30	Figure 15e	0.38	0.002	0.06
Medium	1	15	Figure 15e	0.14	0	0
	1	30	Figure 15a	0.29	0.002	0.09
	3	15	Figure 15e	0.04	0	0
	3	30	Figure 15f	0.05	0	0
Coarse	3	15	Figure 15e	0.24	0	0
	3	30	Figure 15e	0.54	0	0

Note: All experiments were successful with little to no erosion

Sand Erosion

The amounts of collected sand normalized by the experiment surface area are plotted against the XG percentage in the mix and the slope angle in Figure 16 and Figure 17 to understand erosion better. The overall trend indicates that XG percentage increase better stabilizes slopes, and more XG is needed at higher angles and finer sands. Furthermore, erosion susceptibility in treated fine sands is problematic due to the random development of unfavorable surface morphologies. For example, Figure 16a shows that although most experiments at 1% to 3% XG-sand mix cured for 24 hours develop different levels of sliding ridges, the measured erosion is still significantly reduced compared to the pure hydrophobic sand experiments. However, fine sand with 24 h cured 2% XG at 25° performs poorly (Figure 16b). Top Figure 16b shows how the cured protective layer above the pure hydrophobic sand is being compromised as a piece of the crust breaks away. The water that continuously rains and flows down the slope chips away pieces at the exposed location, increasing the size of the sliding patches. From the slope angle perspective, slopes above 20° enhance erosion in cured XG-sand, including all fine sands regardless of the XG percentage, and medium sand with 3% XG. Furthermore, interesting connections exist between the observed surface morphology and erosion rates. For the coarse sand, the sand runoff at a 20° slope was 0.64 mg/cm^2, while the 25° slope yielded no collected erosion. The 20° coarse slope experienced no unusual surface morphology, while the zero-erosion 25° slope formed ridges (Table 3). Unlike a whole section pulling down and forming ridges, tiny particles break out of XG bonds and roll, leading to no sliding ridge formation. Also, while the collected erosion was higher at the 20° than 25° slope, it was only 4.16 g, an amount of no concern. The same phenomenon is seen with medium sand at a 25° angle using a mix of 1% XG, with the surface forming sliding ridges and collecting no erosion. Figure 17b also shows that the medium and fine sands follow a parallel trend, increasing the collected sand runoff by 0.95 mg/cm2 when changing the slope from 20° to 25°,

also connected to the surface morphology illustrated with Figure 17b. Many sliding ridges form on the medium sand experiment with less erosion than coarse sand. The surface morphology changes at the same angle that the coarse sand experiences a shift from sliding ridges to sliding patches. Though fine sand does not develop ridges throughout most of its surface, a tiny patch erodes at the bottom right of the slope. Ridge development allows less sand runoff because sand particles that roll downhill now have a stronger cohesive force from the cured XG. However, after continued rain at high intensities, the stronger crust bonds turn from solids to gooey, and the ridges run the risk of evolving into sliding patches. Based on this, curing a sand mix with 3% XG and developing ridges decreases the amount of sand runoff but can lead to sliding patches and elevated erosion.

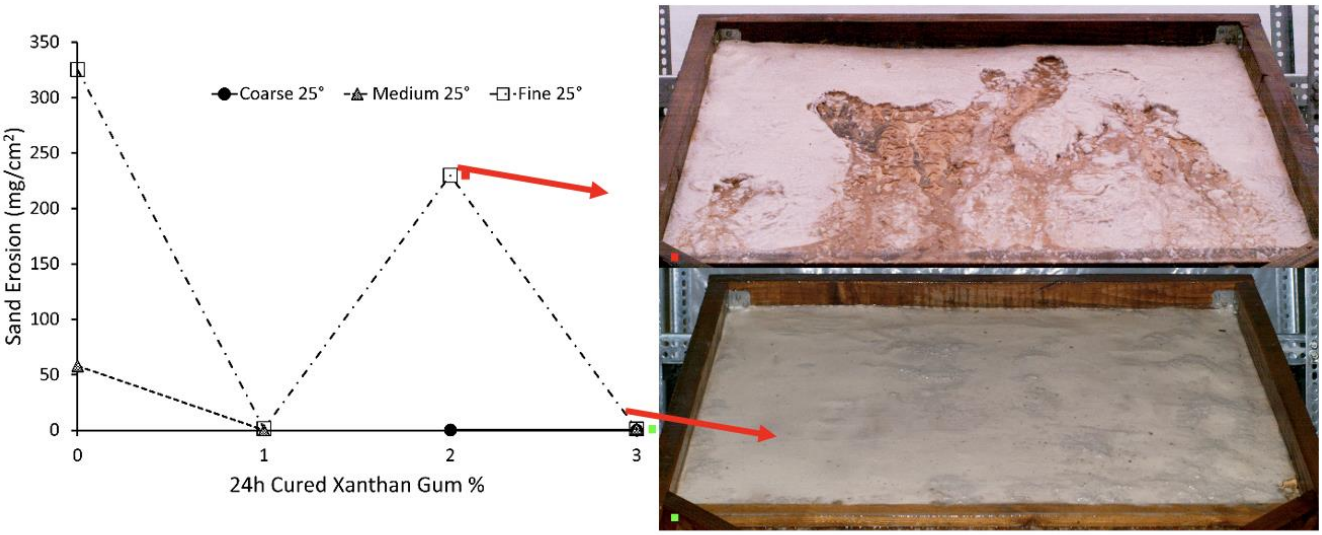

a. Corresponding symbol and colors for reference image data points

b. 24h cured fine sand at 25°. *Top:* 2% XG *Bottom:* 3% XG

Figure 16. Sand erosion with the cured X.G.-sand mix for varying slope angles for 50 mm/hr rain intensities

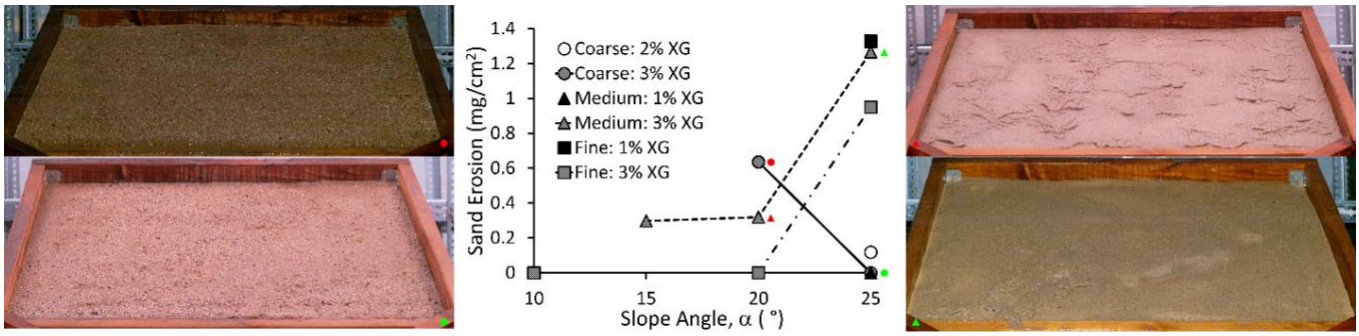

a. 24h cured 3% XG coarse sand. *Top:* 20° *Bottom:* 25°

b. Corresponding symbols and colors for reference image data points

c. 24h cured 3% XG medium sand. *Top:* 20° *Bottom:* 25°

Figure 17. Sand erosion with slope angle for 24h cured XG percentages for 50 mm/hr rain intensities

Water Runoff

Figure 18 shows conclusive results at the highest slopes of 25° for all sand types and percentages of XG and relatively inconclusive results at less steep angles. The water runoff is most increased at 25° and cured 3% XG sand mix over coarse, medium, and fine sand slopes. The water runoff remains roughly the same at untreated to 1% XG as the surfaces formed vertical channels and sliding patches. Furthermore, the water runoff slightly increases at 2% XG as the surface develops larger sliding patches. Finally, the water runoff decreases sharply between 2% to 3% XG for fine sand once the surface forms small sliding ridges. Figure 18b also shows the difference in surface morphology between the fine sand slopes with 3% XG at 25°. The 10° slope at the top of Figure 18b has no surface morphology changes and yielded a much higher water runoff, while the 25° slope has small sliding ridges and experienced a reduced water runoff

Figure 19 shows an inverse relationship between the water runoff and the sand erosion for slopes covered with medium cured 3% XG-sand mix. When the medium sand erosion is lower for the shallower slopes, around 0.3 mg/cm^2, the water runoff is 1.15 mL/cm^2. However, once the medium sand erosion increases to 0.95 mg/cm^2, the water runoff significantly decreases to 0.23 mL/cm^2.

Coarse and fine sand experiments show a slight water runoff increase with an increasing slope, regardless of sand erosion. This idea is depicted in Figure 20, which when looking at a 25° slope, there were coarse, medium, and fine sand trials with cured XG percentages where there was no or little erosion and a water runoff range of 0.02 mL/cm^2 to 0.73 mL/cm^2. A majority of these no erosion data points are below 0.30 mL/cm^2. To conclude, although the water runoff can be high without erosion, both water and sand runoff increase exponentially once the erosion starts.

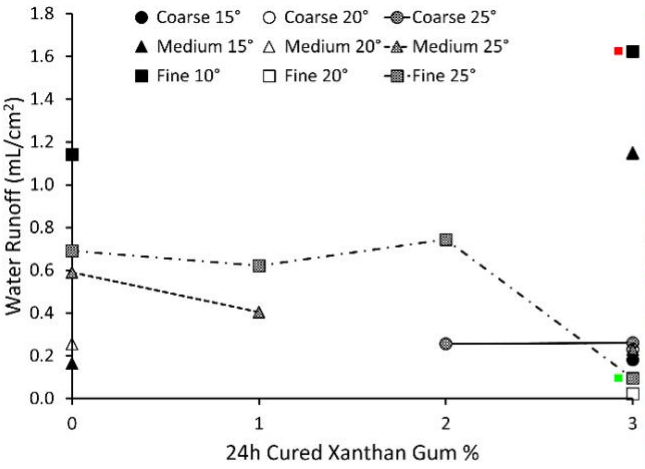

a. Corresponding symbol and colors for reference image data points

b. 24h cured 3% XG fine sand. *Top:* 10° *Bottom:* 25°

Figure 18. Water runoff with 24h cured XG percentage for varying slope angles

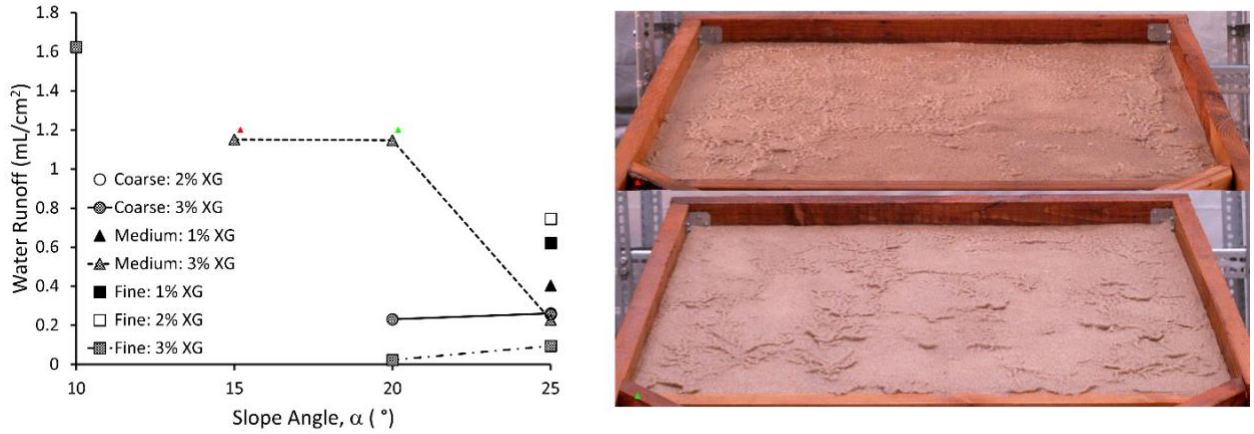

a. Corresponding symbol and colors for reference image data points

b. 24h cured 3% XG medium sand. *Top:* 15° *Bottom:* 20°

Figure 19. Water runoff with slope angle for varying 24h cured XG percentages

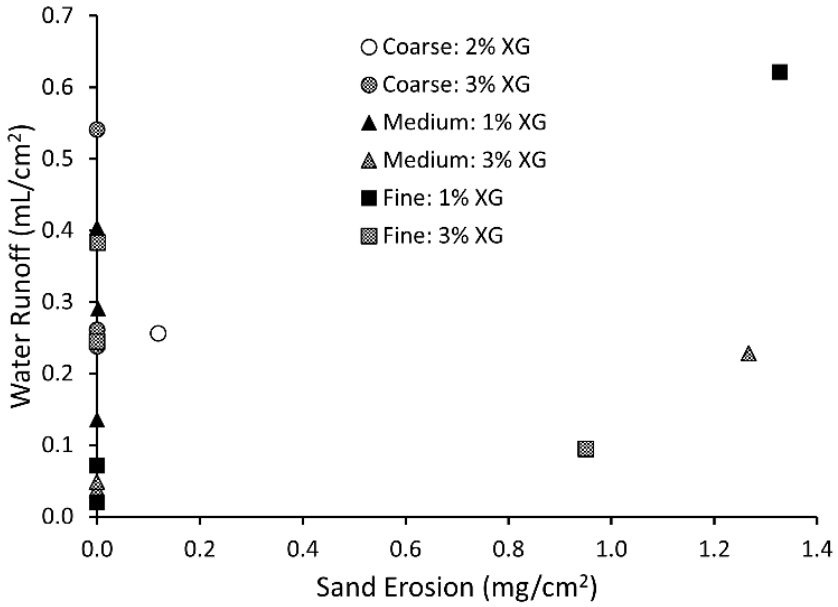

Figure 20. Water runoff with sand runoff for 24h cured XG percentages at a 25° angle

Rain Intensity Effect

Figure 21 shows the sand and water erosion trends, as the rain intensity increases from 15 mm/hr to 50 mm/hr at the steepest slope of 25°. The tested XG percentages for each sand show no sand erosion at 15 mm/hr low rain intensity (Figure 21a, Table 4). At the higher rain intensity of 50 mm/hr, 3% XG controls erosion better than the 1% counterparts overall, except for the experiment in medium sand. Furthermore, 3% XG overall shows less water runoff sensitivity to rain intensity, although there are some variations between sands (Figure 21b). Interestingly, cured fine sand with 1% XG has the lowest water runoff at lower rain intensities but

increases the most as the rain intensity increases, shown in Figure 21b, indicating high erosion potential to turn catastrophic in fine sands, even when improved with XG. Finally, cured coarse sand with 3% XG is relatively insensitive to rain intensity.

Raining duration changes surfaces morphology, erosion, and water runoff. Looking at Figure 22, the lower intensity of the 20 mm/hr experiment is without erosion after the initial 15 minutes. Still, between 15 and 30 minutes, there is erosion, and a few sliding patches fail in both the 1% medium and the 3% fine sand, while the 1% fine and 3% coarse and medium remain uneroded. Figure 22b shows how the surface morphology could change as the rain duration increases. The example shows that the erosion stems from the developed ridge, even though it is small. Much like seen in the previous section, when the surface morphology type changes from ridges to another kind, there is an increase in sand runoff. On the contrary, Figure 23 shows that the water runoff for the lower rain intensity of 15 mm/hr remained consistent with little change in slopes for the duration of the experiment. The higher the XG percentage, the lower the water runoff for cured medium sand. For cured fine sand, the higher the XG percentage, the higher the water runoff, and the most water runoff comes from cured coarse sand with 3% XG.

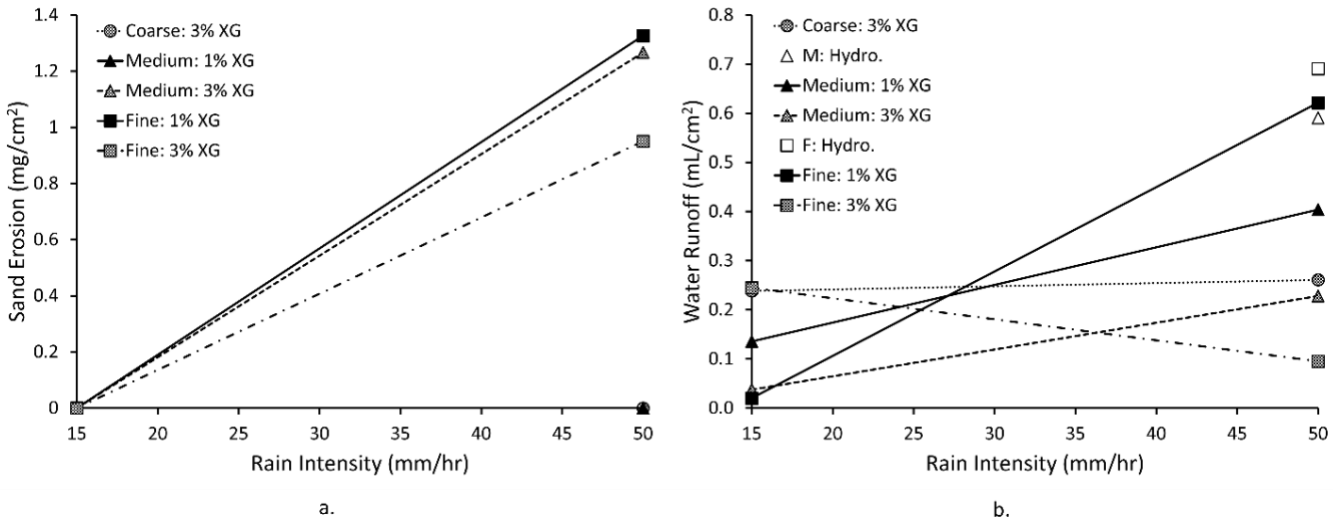

Figure 21. a) Sand runoff with rain intensity at a 25° angle, b) water runoff v. rain intensity at a 25° angle

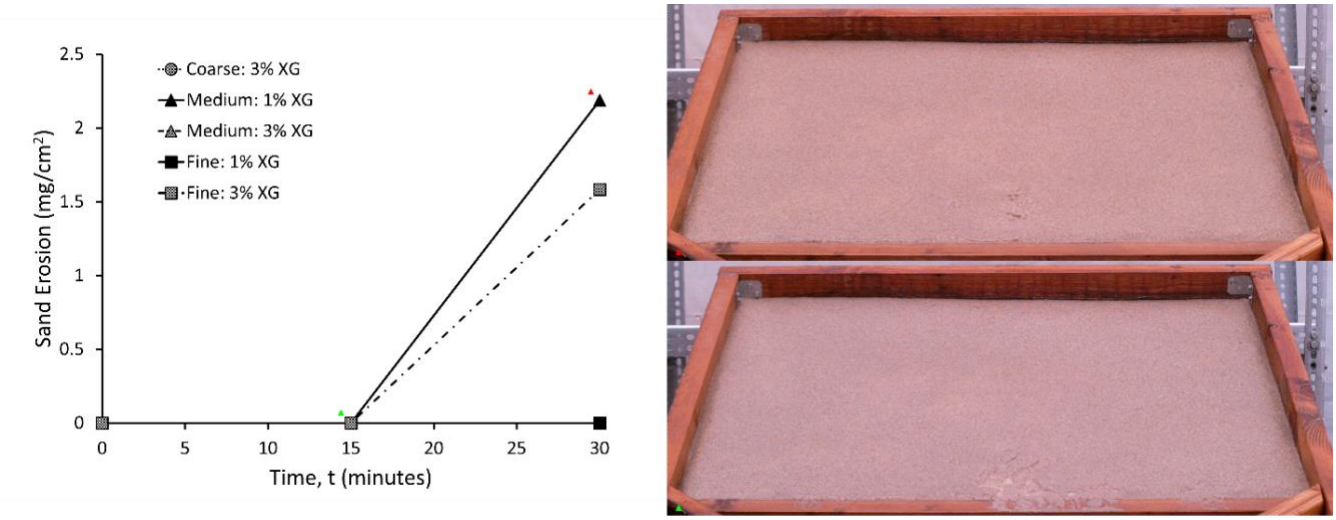

a. Corresponding symbol and colors for reference image data points

b. 24h cured 1% X.G. medium sand at 25°. *Top:* 15 min *Bottom:* 20 min

Figure 22. Sand runoff with time for rain intensities of 15 mm/hr at a 25° angle

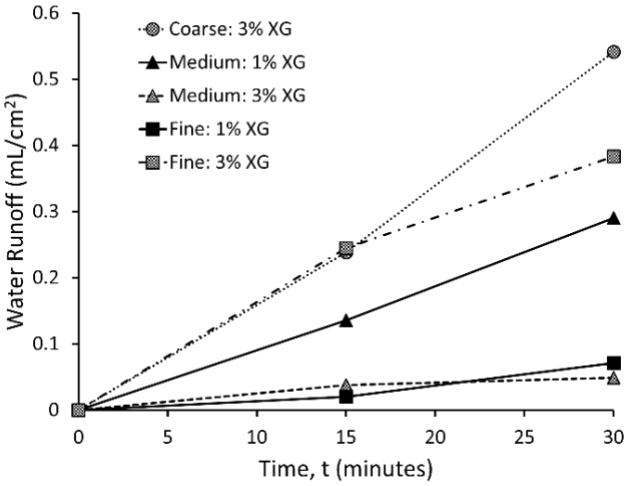

Figure 23. Water runoff with time for rain intensities of 15 mm/hr at a 25° angle

Environmental Aspects of Xanthan Gum Stabilized Slopes

Experimental Setup and Methodology

A total of six slope beds were created out of wood, two beds for each sand type angled at 17° and 21°. Each bed has two flumes with inner dimensions of 43.8 cm in width and 182.9 cm in length. Measuring through critical surface tension, Huffman et al. (2001) found soil hydrophobicity to be stronger at the surface and dissipate as the depth increases, with the last relevant depth further analyzed being 6 cm. According to these findings, the flumes were then pluviated, seen in Figure 24a, with the sand layers seen in Figure 24b to mimic a similar effect of the soil depths. A roller system and wheel guides with a horizontal support system allow sliding ability to keep a constant drop height while pluviating the sands.

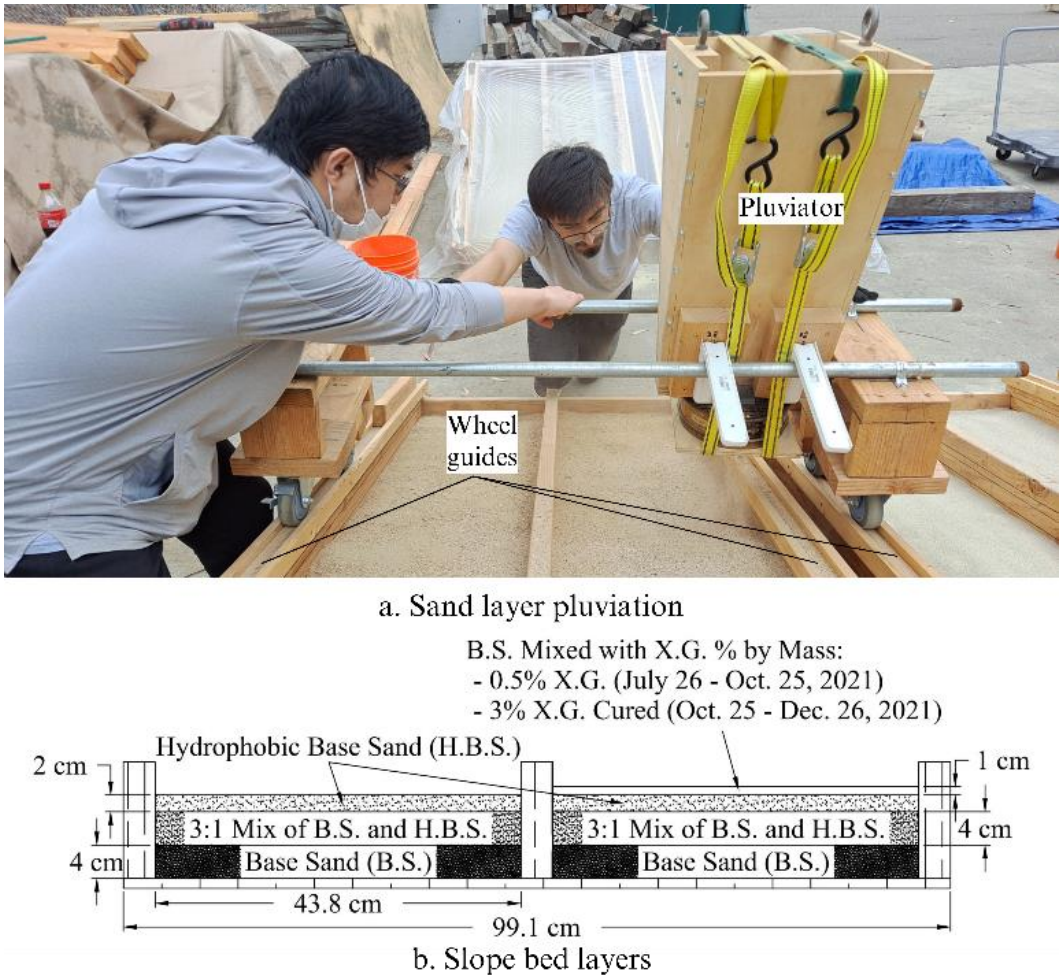

Figure 24. Experiment preparation and layers

The bottom of the slopes contained a wood barrier to support the bottom layers while allowing the top layers with hydrophobicity and the XG treatment to be collected in a catchment, allowing for erosion and water overflow to be measured after rain events. The left flume on each slope bed contained unmitigated hydrophobic sand, while the right flumes had the XG treatment. The initial treatment of the slopes had 0.5% concentration by mass of XG mixed with the base sand. The first seven rain events used this percentage. On November 21, 2021, the treated slopes were re-covered using 3% concentration by mass of XG mixed with the base sand and cured by spraying the layer with 16.5% by mass of water, that formed a hardened crust layer after drying.

Erosion and Water Overflow Results After Seven Rain Events

Initially, the hydrophobic base sand on the right flume of each slope bed was covered with 1 cm of the base sand mixed with 0.5% XG (Figure 25). Throughout the 6-months duration of the experiment, leaves, twigs, and

bark from the surrounding trees landed on the slopes, and a family of raccoons occasionally stepped on the slopes. With all these external factors commonly occurring in nature, these experiments paired with natural rain events (RE) provide results for real-world performance of hydrophobic slopes post-treatment for coarse, medium, and fine sand. Table 5 summarizes the nine REs occurring over the span of July 26, 2021, to December 26, 2021 with data courtesy of MesoWest from the University of Utah (https://mesowest.utah.edu/). Stations E3170 and F8273 are located 1.85 km and 3.27 km, respectively, from the experiment locations. Table 6 contains the erosion and water runoff normalized by the projected surface area for each slope, sand type, and RE.

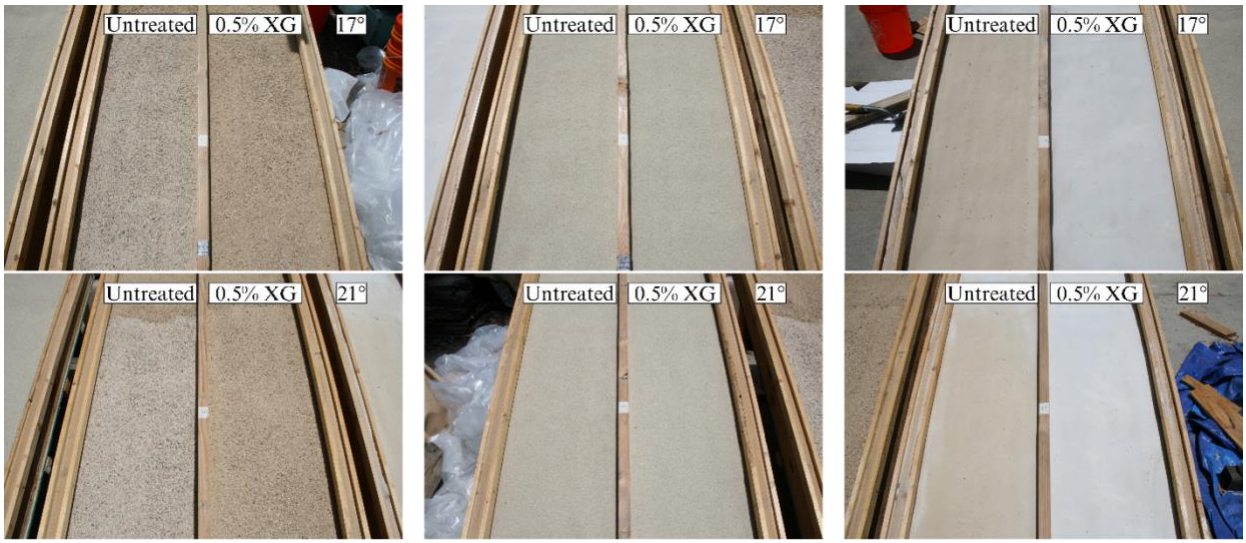

a. Coarse sand b. Medium sand c. Fine sand

Figure 25. Slope beds after placement

Table 5. Data and slope treatment type for each rain event courtesy of MesoWest from the University of Utah (https://mesowest.utah.edu/)

RE	Date	Station ID	Duration (min)	Avg. *i* (mm/hr)	Max. *i* Time (PST)	Max. *i* (mm/hr)	Treatment Type
1	7/26/2021	E3170	75	0.76	4:45 - 5 a.m.	2.03	U
2	8/11/2021	E3170	31	0.49	4 - 4:31 a.m.	0.49	U
3	9/9/2021	E3170	29	5.78	8:02 - 8:17 p.m.	9.14	U
4	9/27/2021	E3170	464	0.29	6:01 - 6:15 a.m.	1.09	U
5	10/5/2021	F8273	435	1.40	1:31 - 1:46 a.m.	4.06	U
6	10/8/2021	F8273	225	1.02	4:46 - 5:01 a.m.	3.05	U
7	10/25/2021	F8273	151	1.69	4:31- 4:46 p.m.	11.18	U
8	12/14/2021	E3170	750	2.84	12 - 12:15 p.m.	14.22	C
9	12/26/2021	E3170	166	1.52	2:31 - 2:45 a.m.	14.15	C

Note: RE = rain event; *i* = rain intensity; U = uncured 0.5% XG; C = cured 3% XG

Table 6. Normalized erosion and water runoff values for each sand type, angle, and treatment type after rain events

			Coarse				Medium				Fine			
			17°		21°		17°		21°		17°		21°	
	RE	TT	w/o XG	w/ XG%	w/o XG	w/ XG%	w/o XG	w/ XG%	w/o XG	w/ XG%	w/o XG	w/ XG%	w/o XG	w/ XG%
Erosion (mg/cm²)	1	Uncured 0.5% XG	0.42	0.45	0.59	0.55	0.61	0.39	1.23	1.30	0.68	0.83	0.94	0.85
	2		0.18	0.05	0.12	0.09	0.12	0.05	0.40	0.09	0.28	0.22	0.32	0.26
	3		6.38	2.11	2.95	5.60	97.63	69.16	49.33	31.79	216.82	219.34	293.37	339.71
	4		0.44	0.07	0.13	0.02	0.94	0.30	0.37	0.37	2.12	0.42	1.20	0.90
	5		3.79	5.99	1.79	4.94	5.50	56.31	5.71	77.61	46.21	140.46	58.72	64.26
	6		1.36	0.76	0.21	0.48	0.70	0.86	0.77	2.20	0.90	1.21	1.54	1.75
	7		1.08	0.84	1.14	0.35	3.37	11.95	3.26	20.01	88.05	67.62	114.23	95.16
	8	Cured 3% XG	1.33	1.10	2.19	1.92	6.65	15.48	8.50	12.41	120.31	28.31	34.63	32.84
	9		3.85	1.85	2.19	6.11	6.65	129.65	6.66	93.06	75.95	196.58	86.47	209.98
Water runoff (mL/cm²)	3	Uncured 0.5% XG	10.33	44.86	22.26	90.59	14.87	35.79	44.77	234.86	37.05	46.62	73.31	80.90
	4		2.15	5.41	0.36	0.56	0.33	0.89	0.61	0.36	0.59	0.57	0.60	0.05
	5		31.86	97.20	21.72	112.51	0.68	138.86	139.84	681.79	14.37	52.42	99.49	131.44
	6		0	0	0.07	0	0	0	0	6.11	0	0	0	0.01
	7		3.44	0.24	2.36	0.24	8.34	11.59	106.30	56.03	40.07	18.65	80.90	23.30
	8	Cured 3% XG	703.40	408.78	15.71	735.20	132.82	1341.02	94.52	1160.67	457.17	307.22	820.82	306.60
	9		25.71	430.20	46.08	474.43	44.36	1348.33	111.54	1142.87	95.01	1004.06	131.44	1004.36

Note: RE = rain event; TT = treatment type; All values are normalized against the projected slope surface

Surface Morphology Throughout Rain Events

The first two REs did not cause significant changes to the slopes as the rain durations were short and the rain intensities were low. The initial RE 1 rain wetted the XG coating on the sand particles and formed a hardened crust layer. After RE 2, raccoons walked along the surface of two slopes: the treated coarse slope, and the untreated fine slope, both at 17°. The treated coarse sand was not largely affected by animal footprints. Still, the untreated fine sand contained a section of the displaced hydrophobic layer, exposing the less hydrophobic layer underneath. However, this did not affect the overall trends of the erosion, as the 17° fine slopes data in Table 6 reveal that the 0.5% XG flume still experienced higher erosion than its untreated counterpart during RE 3 and the treated coarse sand had less erosion.

a. Coarse sand b. Medium sand c. Fine sand

Figure 26. Surface morphology after RE 3 on September 10, 2021

RE 3 with a max. 15-min rain intensity of 9.14 mm/hr caused the first significant change in surface morphology, leading to a larger erosion yield for each slope and sand type. Figure 26a, Figure 26b, and Figure 26c depict the surface morphology changes when comparing the sand types. Coarse slopes showed minor changes. Some channels began to form on medium slopes, while deep channels already formed on fine slopes. As the rain events continued, the channels seen in the fine sand slopes became more prevalent and extremely large (Figure 27a). With a cured layer from the XG after continuous rain, more raccoon activity broke apart the surface layer and created more drastic surface conditions exposing the hydrophobic layers susceptible to mudflows (Figure 27b).

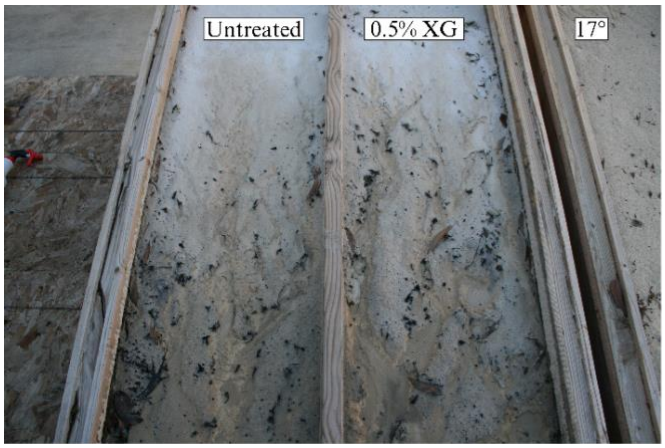

a. Fine sand morphology after RE 7

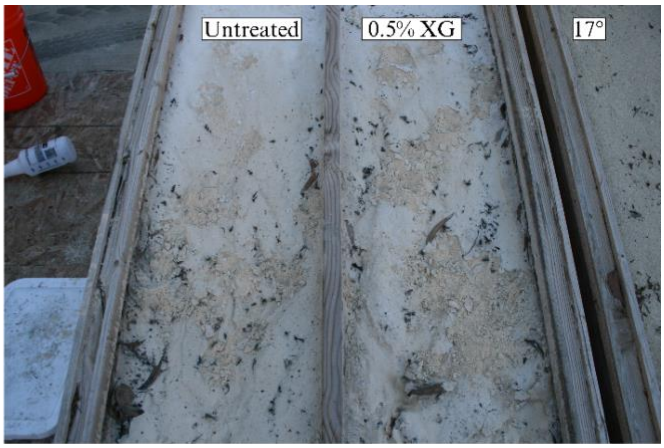

b. Raccoon prints prior to re-covering the slopes

Figure 27. Extreme channels formed in the fine sand slope with subsequent animal activity

Concurrent experiments with simulated rainfall had shown that a cured 3% XG-sand mix significantly reduced erosion at rain intensities of 15 and 50 mm/hr, so the performance of this solution when pluviated from above onto eroded slopes was tested for real-world applications (Figure 28 and Figure 29). Comparing the images before re-covering with the corresponding surface morphology after RE 8 in Figure 30 reveal that the erosion followed the same pattern, with most of the flow diverting into the pre-formed channels and chipping away the cured layer at those sections. Figure 30 also shows the state of the slopes during the last two REs. The surface morphology was not the only factor that lead to enhanced erosion, as Figure 30b reveals that the XG treated flume had still not dried seven days later, three days before RE 9 with a rain intensity of 14.15 mm/hr and a rain duration of 166 min, shorter than RE 8 by 584 min, due to the higher XG percentage and the colder temperature observed in December. With the slopes over-wetted, the hardened crust layer remained in a gel state, allowing entire sections along the pre-existing channels to erode swiftly. Figure 31 shows the final surface morphology of each slope.

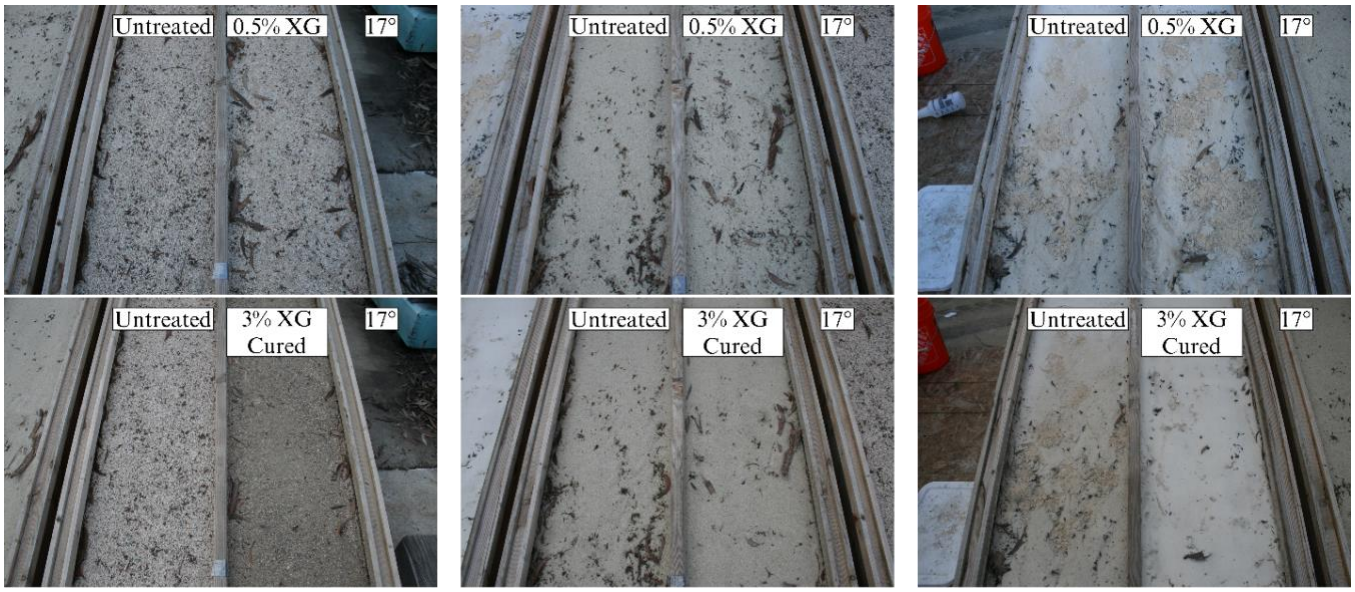

a. Coarse sand b. Medium sand c. Fine sand

Figure 28. 17° slopes before (top) and after (bottom) re-covering with cured 3% X.G on November 22, 2021

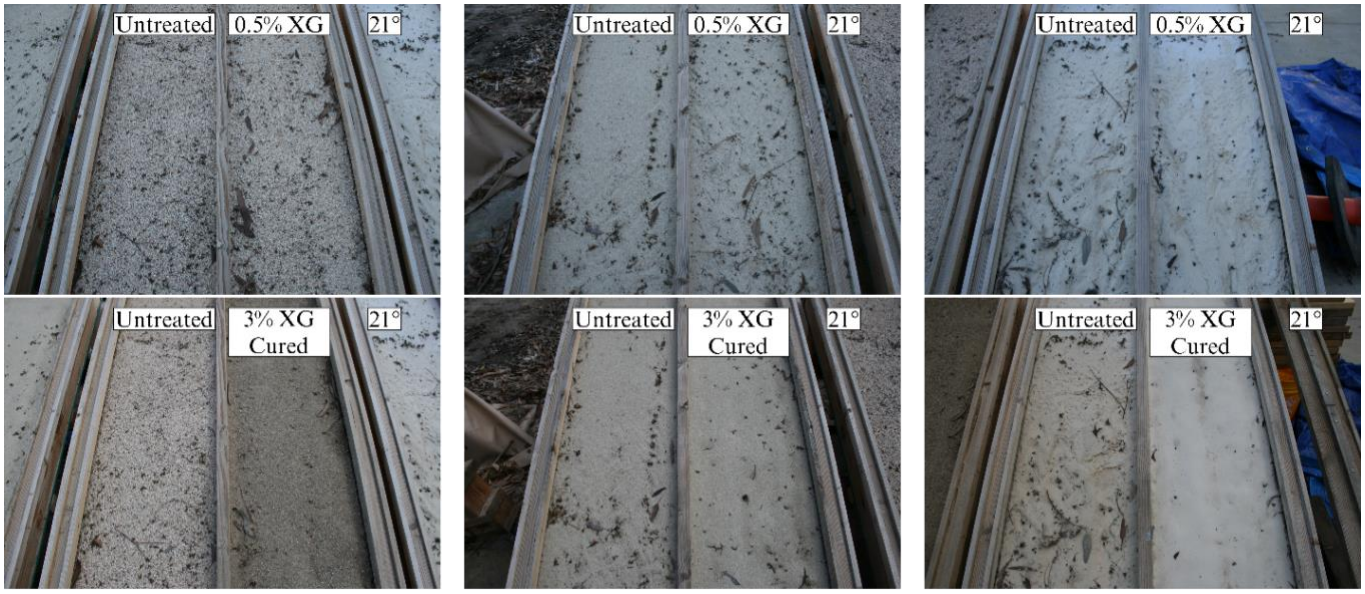

a. Coarse sand b. Medium sand c. Fine sand

Figure 29. 21° slopes before (top) and after (bottom) re-covering with cured 3% X.G. on November 22, 2021

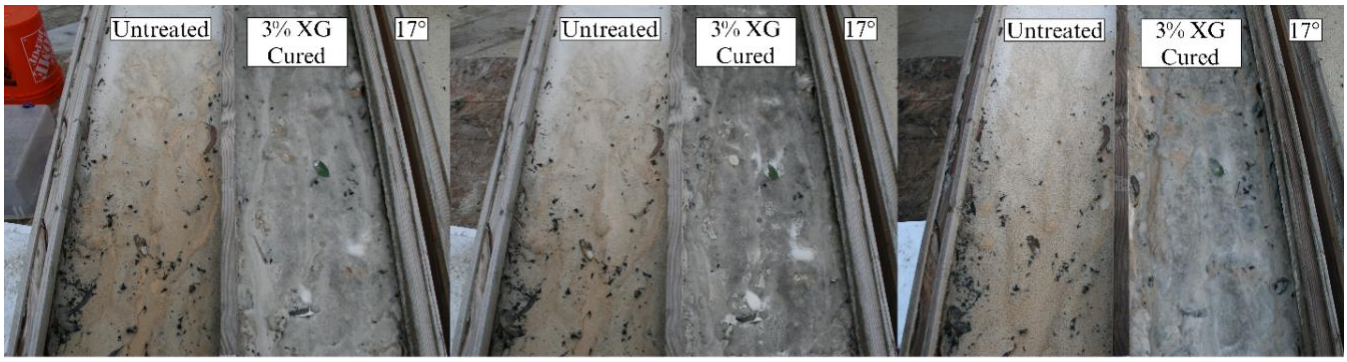

a. December 16, 2021, after RE 8 b. December 23, 2021, 3 days before RE 9 c. December 27, 2021, after RE 9

Figure 30. Enhanced erosion at pre-existent channels and over-saturated XG-sand mix

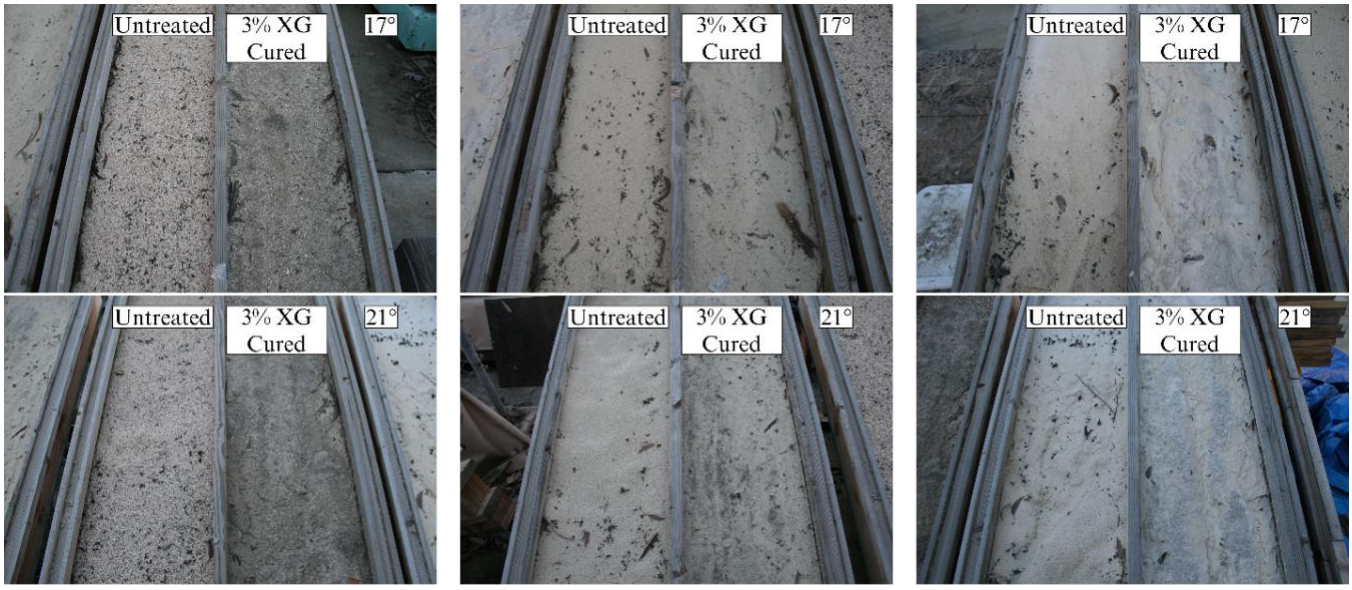

a. Coarse sand b. Medium sand c. Fine sand

Figure 31. Final surface morphology on February 4, 2022

Erosion and Water Runoff

As shown in Table 5, real-world rainstorms are uncontrolled events with the rain duration, average and 15-min peak rain intensities varying widely. Because the rain variables change from one storm to the next, erosion and water runoff may be assumed not to follow a trend. Still, when plotting the 15-min peak rain intensities and erosion (Figure 32a) and water runoff (Figure 32b), they both follow the trend of the rain intensities regardless of the duration it rained. After the slopes are re-covered, however, this ceases to be the case.

As for the treatment performance, Figure 32a shows that the 0.5% XG treated flumes for both fine sand slopes did not reduce erosion compared to the untreated slopes, with the angles 21° and 17° eroding even more for

the angles RE 3 and RE 5, respectively. On these same REs, the water runoff for the treated flumes was also slightly more than observed for the untreated slopes. Once re-covered with the cured 3% XG-sand mix, the 17° treated slope performed much better, with 28.31 mg/cm^2 eroded instead of 120.31 mg/cm^2 from the untreated flume during RE 8, while the 21° performed only slightly better. The final RE saw a large increase in erosion for the XG-covered slopes and an even larger increase in water runoff.

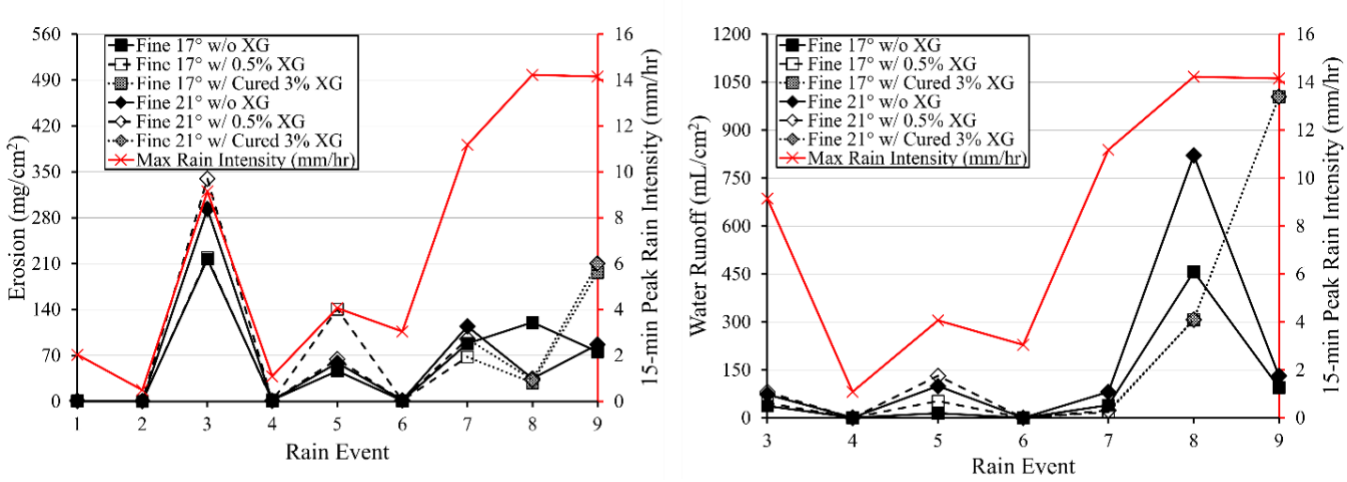

a. Erosion recorded for each rain event

b. Water runoff recorded for each rain event

Figure 32. Fine sand erosion and water runoff with the 15-min peak rain intensities

For medium sand shown in Figure 33, the 0.5% XG slopes have reduced erosion during RE 3, but experience much more erosion in RE 5, with the 17° slope experiencing 10.2 times more and the 21° slope with 13.6 times more, than the untreated slopes. The same trend is seen with the water runoff. After RE 3, there was little erosion in the untreated hydrophobic slopes. The water runoff stayed consistent with an increase, decrease, and another increase from RE to RE. After applying the cured 3% XG treatment, the erosion decreased or stayed the same at a higher rain intensity than before, but it did not reduce the erosion to be less than the untreated slopes. The treated slopes then see a spiked increase in erosion during RE 9, much like the fine sand treated slopes. This is explained by the pre-formed channels from before the slopes were re-covered, with the enhanced erosion occurring along those channels. Recall Figure 30b, showing the slopes were not completely dry from RE 8 when RE 9 occurred, leading the already saturated XG-sand mix to slide down in pieces instead of a hardened crust protecting the slope before being over-wetted.

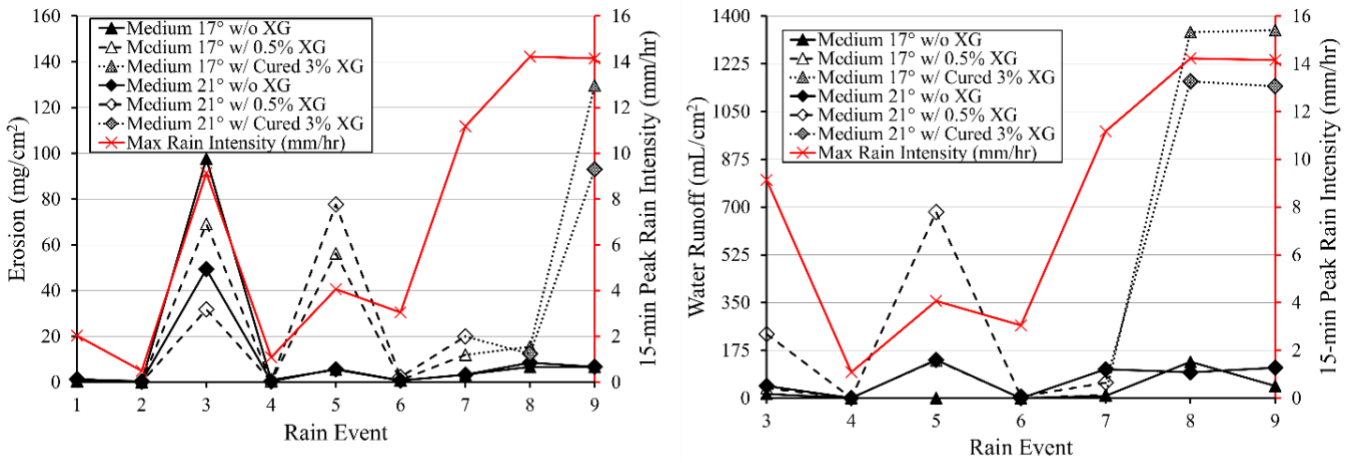

a. Erosion recorded for each rain event

b. Water runoff recorded for each rain event

Figure 33. Medium sand erosion and water runoff with the 15-min peak rain intensities

Figure 34a shows that the 0.5% XG 17° initially reduced erosion during RE 3, but produced more during RE 5, much like was seen with the medium sand treated slopes. Both treated angles yielded less erosion than the untreated slopes during RE 7 and continued that trend after re-covering with cured 3% XG. Once again, there was an increase in erosion from RE 9, but not to a large extent as the largest increase was in the 21° treated slope, from 1.92 to 6.11 mg/cm^2. During REs 3, 5 and 9, the water runoff produced from the treated slopes were higher.

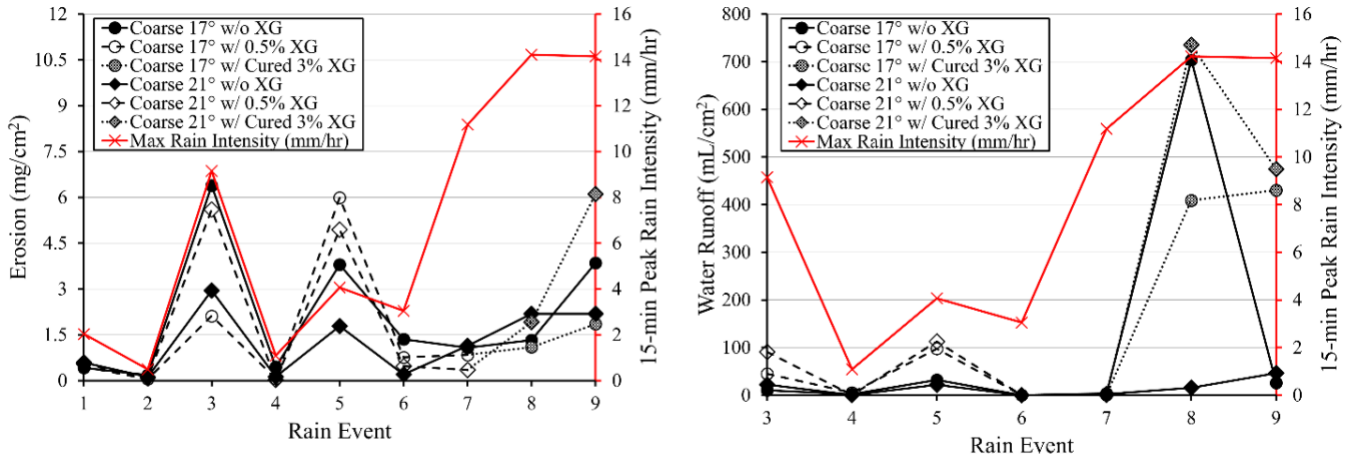

a. Erosion recorded for each rain event

b. Water runoff recorded for each rain event

Figure 34. Coarse sand erosion and water runoff data with the 15-min peak rain intensities

Cumulative Erosion and Water Runoff

Figure 35, Figure 36, and Figure 37 compare the cumulative erosion and water runoff for each angle and treatment type for fine, medium, and coarse sand. Focusing on the cumulative erosion for each sand type, the most erosion with the 0.5% XG treatment for fine sand occurred during RE 3 and RE 5 for medium and coarse sand. As seen with the data collected each RE, the cumulative erosion shows the similarities in erosion trends when XG is used. For all sand types and both angles, the XG treated slopes follow the same trends but at different values, with the fine sand slopes eroding the most with a cumulative erosion of 700.35 mg/cm^2 averaged between the angles, coarse sand slopes the least with 16.63 mg/cm^2, and medium sand slopes eroding in-between the two with 261.50 mg/cm^2. However, the untreated hydrophobic slopes do not have similar trends between each sand, except for the erosion from RE 3. While the cumulative figures show the untreated fine sand erosion increases from RE to RE with different slopes, the coarse cumulative trend is more linear. It can also be seen that after the initial erosion from RE 3, medium sand erosion is very little and very linear.

When comparing the cumulative water runoff for each sand, once again it can be seen that the water runoff follows a similar trend from sand to sand for untreated and 0.5% XG treated slopes, with the 0.5% XG 21° slope producing more overall water runoff during REs 3 and 5 but maintain the same trend. When the XG is increased to 3%, much higher water runoff was observed. It can be noted that the water runoff slopes between REs 8 and 9 go from steeper, linear, and shallower from fine to medium and to coarse sands. This is explained through the saturation of the slopes, where most of the fine sand slope was still over-saturated from the previous RE, and the coarse sand slopes were the least over-saturated slopes, allowing the XG-sand mixture to absorb water, producing less water runoff. For the XG treated slopes, those with medium sand accumulated the most water runoff, with 3079.58 mL/cm^2 averaged between the angles, fine sand slopes less than half of the medium slopes producing 1488.10 mL/cm^2, and the least were coarse sand slopes with 1200.11 mL/cm^2.

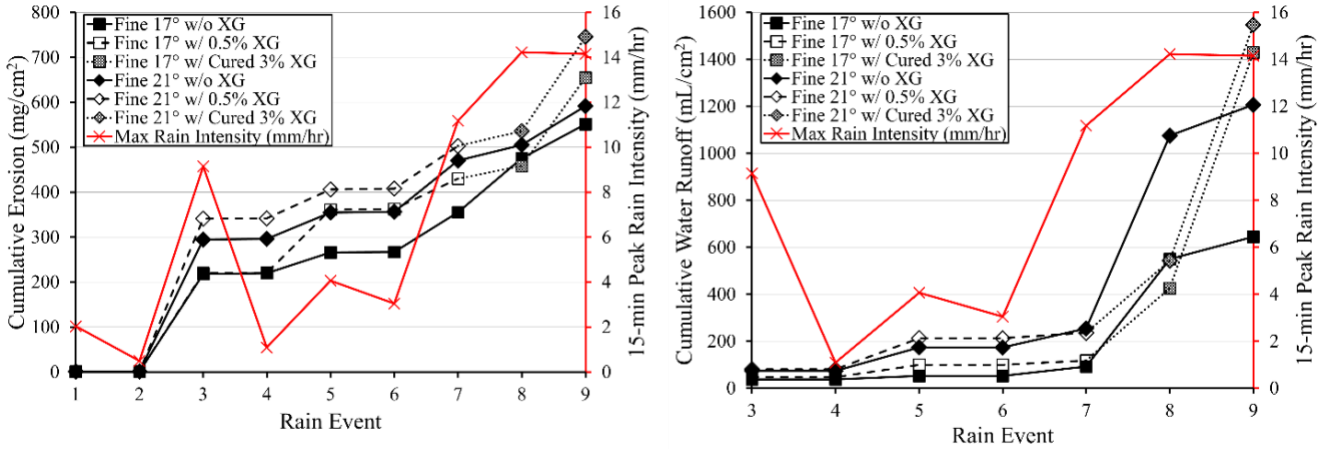

a. Cumulative erosion after each rain event

b. Cumulative water runoff after each rain event

Figure 35. Fine sand cumulative erosion and water runoff with the 15-min peak rain intensities

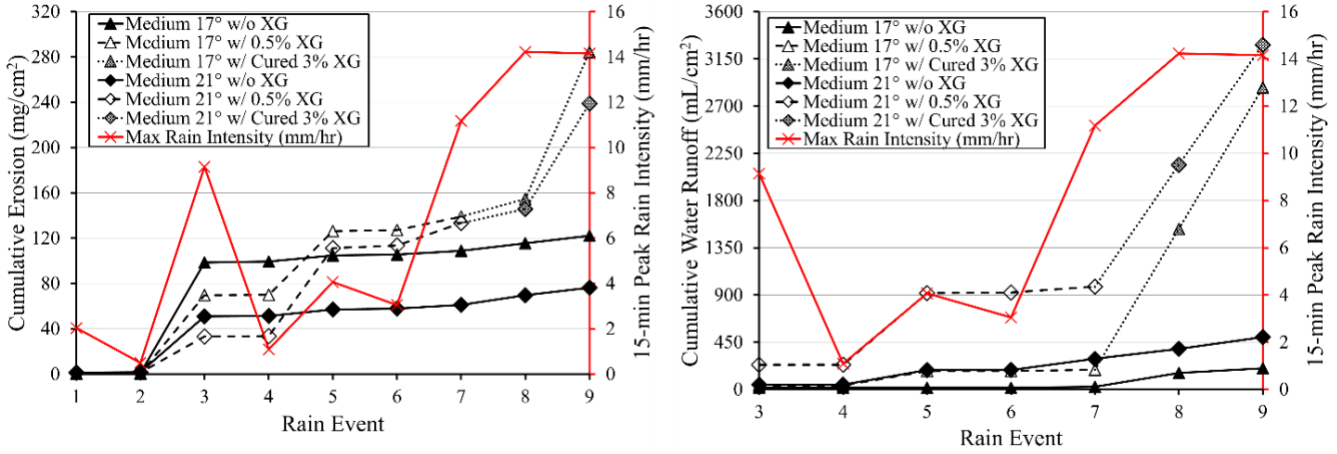

a. Cumulative erosion after each rain event

b. Cumulative water runoff after each rain event

Figure 36. Medium sand cumulative erosion and water runoff with the 15-min peak rain intensities

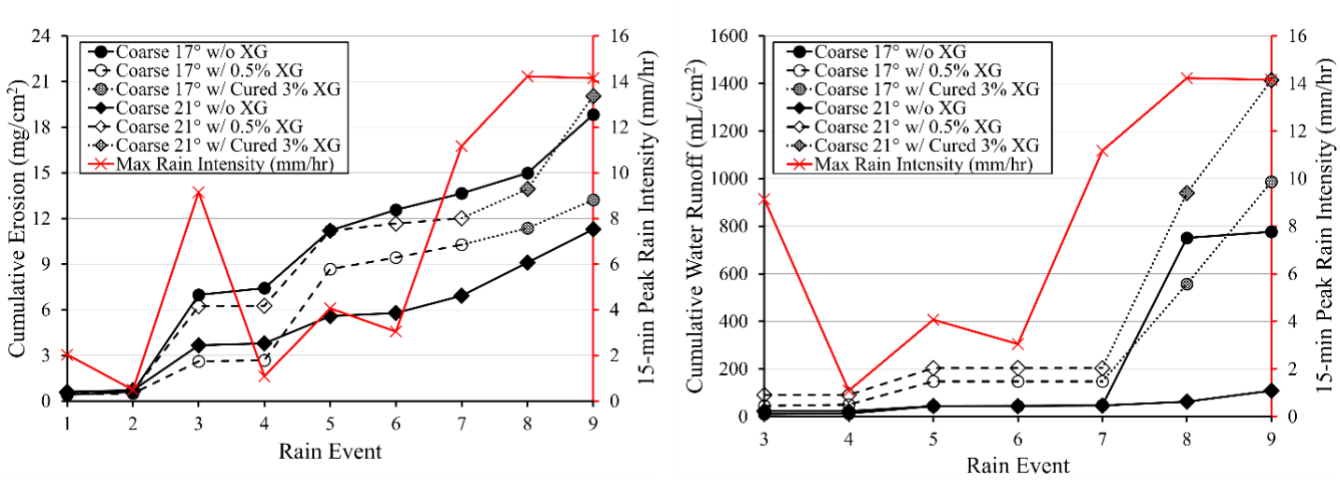

a. Cumulative erosion after each rain event

b. Cumulative water runoff after each rain event

Figure 37. Coarse sand cumulative erosion and water runoff with the 15-min peak rain intensities

Conclusions and Recommendations

Wildfire frequency has been increasing in recent years, posing more threats to the environment, people, and civil infrastructure not only because of burning but also post-wildfire mudflows. Burned scars are more susceptible to mudflows, and debris flows when rain falls onto slopes that lost vegetation and whose surficial soil layers turned hydrophobic. This paper explored the advantages and limitations of surficial soil improvement of burned scars with biopolymer, specifically Xanthan gum (XG), using various slopes at high and low rain intensities. However, this controlled intermediate-scale study did not necessarily linearly upscale specific findings to natural slopes with varying inclinations and heterogeneous surficial hydrophobicity.

This study concluded that, despite the limited literature, sprinkling surfaces with pure XG did not yield sufficient stability against erosion during prolonged rains. Furthermore, a different technique was proposed that pre-mixes XG and sand in a dry state and then spreads and wets the mix over hydrophobic slopes with drones. The erosion values for each cured experiment were significantly reduced compared to the untreated hydrophobic slopes. Furthermore, this study showed that curing the pluviated sand and XG mix for a day after wetting decreased the sand runoff and kept the water runoff relatively low. However, we classified the surface morphology of treated slopes after the low and high-intensity rain and identified possible pitfalls. Specifically, fine, medium, and coarse severely hydrophobic sand, 10° to 30° sloped surfaces, covered with a layer of XG-sand mix at 1% to 3% mass ratios, were tested under 15 mm/hr and 50 mm/hr rain intensities. The sand mixed with XG was untreated, thus not hydrophobic. Sand coarseness played a significant role in XG erosion control. Low rain intensity 15 mm/hr did not erode slopes with 1% to 3% cured XG mixes across a variety of angles from 10° to 25°, although minor erosion occurred in medium and fine sands covered with 1% XG mix.

Furthermore, at high 50 mm/hr rain intensity, coarse sand performed well at all inclinations when treated with 3% XG and showed only a small amount of erosion with 2% XG. Medium sand, on the contrary, was more sensitive, and although 3% XG performed well at wide slope ranges from 15° to 25°, extreme erosion occurred when the XG percentage was as low as 0.5% at higher angles of 20° and 30°. The transition of medium sand occurred at 25°, where small erosion patches formed. On the other hand, fine sand covered with 3% XG mix performed well at angles 10° to 25°, where small ridges formed at steeper slopes. Furthermore, lower 1% and 2% XG fine sand mixes performed poorly at 25°. Despite surficial improvements, the water runoff can be high without erosion, indicating limited infiltration capabilities. In addition, both water and sand runoff increased exponentially once the erosion started. It is essential to consider the expectancy of the rain because this study shows modified surface morphology formed during the rain event. Some experiments showed the development of ridges that could further erode during rain.

Finally, the first study recommends a practical XG percentage of the mix for slope improvement, relying on results at 25° angle. The surface erosion types were similar for coarse and medium sand, making 2% XG the most material-efficient while having negligible erosion with the same water runoff seen with 3% XG. Finally,

for fine sand, 1% XG has a high likelihood of forming a larger sliding patch the more prolonged the rain duration, so ≥3% XG is recommended.

With natural rain events, debris from trees, and animal activity interacting with the hydrophobic slopes, the second part of the study offers real-world performance after applying XG-sand mixtures as a slope stability mitigation technique. The results validated conclusions from a single controlled rain event study, which found that an uncured 0.5% XG-sand mix produced more erosion than an untreated hydrophobic slope. Furthermore, the environmental research provided insight into the performance of cured 3% XG-sand mixes on slopes with pre-existing channels.

The low rain intensities from REs 1 and 3, which enabled wetting and allowed the surfaces to cure, provided a hardened layer that eroded a similar amount as the untreated slopes and provided more water runoff due to reduced infiltration from the XG bonds. With a higher percentage of XG used to give stronger bonds between the particles, the initial rain events would produce less erosion and more water runoff due to the higher concentration of XG filling gaps between the particles.

While cured 3% XG-sand mixes reduced surface erosion for non-eroded slopes, the presence of pre-existing channels dramatically increased erosion. Therefore, XG application on burned slopes in nature, with channels already from previous erosions, can be significantly at risk. If surficial channels are present, we recommended using percentages larger than 3% in the XG-sand mixture. Recommendations must also be used cautiously, considering the frequency of storms in the area and the temperature. For example, with 0.5% XG after RE 5, the slopes were arid three days before RE 6 in early October. However, after 3% XG was applied and after RE 8 in mid-December, 12 days was not enough to completely dry the slopes, resulting in significantly increased erosion during RE 9.

Using XG as a slope stability technique provided fairly similar erosion trends for all three sand types tested, with fine sand slopes eroding the most, medium sand slopes next, and the least was the coarse sand slopes. In addition, very similar trends were found between each sand type for the collected water runoff, with coarse sand slopes producing the least, fine sand slopes slightly more than coarse, and more than double the water runoff in fine sand slopes were observed with the medium sand slopes.

References

Akin, I. D., Garnica, S. S., Robichaud, P. R., Brown, R. E. Surficial Stabilization of Wildfire-Burnt Hillslopes Using Xanthan Gum and Polyacrylamide. Geotech Geoogical Engineering, 2021. DOI: 10.1007/s10706-021-01951-4.

Akin, I. D., and Likos, W. J. Water vapor sorption of polymer-modified bentonites. Proceedings of Geo-Chicago 2016 technical papers, Reston, VA, ASCE, 2016. https://doi.org/10.1061/9780784480144.050.

Alexandre, M., Dubois, P. Polymer-layered silicate nanocomposites: preparation, properties and uses of a new class of materials. Mater Sci Eng, 2000. 28:1–63.

Ayeldeen, M. K., Negm, A. M., El Sawwaf, M. A. Evaluating the physical characteristics of biopolymer/soil mixtures. Arab J Geosci, 2016. 9: 371. https://doi.org/10.1007/s12517-016-2366-1.

Cabalar, A., Wiszniewski, M., Skutnik, Z. Effects of Xanthan Gum Biopolymer on the Permeability, Odometer, Unconfined Compressive and Triaxial Shear Behavior of a Sand. Soil Mech Found Eng, 2017. 54: 356-361. https://doi.org/10.1007/s11204-017-9481-1.

Carvalho, S. C. P., de Lima, J. L. M. P., and de Lima, M. I. P. Using meshes to change the characteristics of simulated rainfall produced by spray nozzles. International Soil and Water Conservation Research, 2014. 2(2): 67–78. DOI: 10.1016/S2095-6339(15)30007-1.

Chen, R., Lee, I., Zhang, L. Biopolymer Stabilization of Mine Tailings for Dust Control. J. Geotech. Geoenviron. Eng., 2015. Volume: 141, 2. DOI: 10.1061/(ASCE)GT.1943-5606.0001240

CNRFC and NOAA (2021). CNRFC Data Archive, <https://www.cnrfc.noaa.gov/arc_search.php>.

Crockford, H., Topalidis, S., Richardson, D. P. Water repellency in a dry sclerophyll eucalypt forest—measurements and processes. Hydrol. Process, 1991. 5: 405-420. https://doi.org/10.1002/hyp.3360050408

DeBano, L. F. Water repellant soils: a state-of-the-art. Gen. Tech. Rep. PSW-46, illus. Pacific Southwest Forest and Range Exp. Stn., Forest Serv., US Dep. Agric., 1981. Berkley, CA; 21.

DeBano, L. F, Krammes, J. S. Water repellent soils and their relation to wildfire temperatures. Bulletin of the International Association of Scientific Hydrology, 1996. 11(2): 14 – 19.

DeBano, L. F., Osborn, J. F., Krammes, J. S., Letey, J. Soil wettability and wetting agents: our current knowledge of the problem. USDA For. Serv. Res. Pap., 1967. PSW-43: 13.

Doerr, S. H., Shakesby, R. A., Walsh, R. P. D. Soil hydrophobicity variations with depth and particle size fraction in burned and unburned Eucalyptus globulus and Pinus pinaster forest terrain in the Aqueda Basin, Portugal. Catena, 1996. 27: 25 – 47.

Doerr, S. H., Shakesby, R. A., Walsh, R. P. D. Soil water repellency: its causes, characteristics, and hydro-geomorphological significance. Earth-Science Reviews, 2000. 51: 33 – 65.

Department of Forestry and Fire Protection (2022). Stats & Events. Cal Fire. https://www.fire.ca.gov/stats-events/

Gioia, F. and Ciriello, P. P. The containment of oil spills in porous media using xanthan/aluminum solutions, gelled by gaseous CO2 or by AlCl3 solutions. Journal of Hazardous Materials, 2006. 138(3) 500–506.

Ham, S.-M., Chang, I., Noh, D.-H., Kwon, T.-H. Improvement of Surface Erosion Resistance of Sand by Microbial Biopolymer Formation. J. Geotech. Geoenviron. Eng, 2018. 144: 7. DOI: 10.1061/(ASCE)GT.1943-5606.0001900

Helvey, J. D. Effects of a north central Washington wildfire on runoff and sediment production. Water Resources Bulletin, 1980. 16(4): 627 – 634

Huffman, E. L., MacDonald, L. H., Stednick, J. D. Strength and persistence of fire-induced soil hydrophobicity under ponderosa and lodgepole pine, Colorado Front Range. Hydrol. Process., 2001. 15: 2877-2892. https://doi.org/10.1002/hyp.379

Joga, J.R. and B.J.S., V. Effect of xanthan gum biopolymer on dispersive properties of soils. World Journal of Engineering, 2020. 17(4): 563-571. https://doi.org/10.1108/WJE-05-2020-0152

Kavazanjian, E., Iglesias, E., Karatas, I. Biopolymer soil stabilization for wind erosion control. Proceedings of the 17th International Conference on Soil Mechanics and Geotechnical Engineering: The Academia and Practice of Geotechnical Engineering, 2009. 1: 881-884. https://doi.org/10.3233/978-1-60750-031-5-881

Khachatoorian, R., Petrisor, I. G., Kwan, C.-C., Yen, T. F. Biopolymer plugging effect: laboratory-pressurized pumping flow studies. Journal of Petroleum Science and Engineering, 2004. Volume: 38 (1-2): 13–21.

Lee, S., Im, J., Cho, G.-C., and Chang, I. Laboratory triaxial test behavior of xanthan gum biopolymer-treated sands. Geomechanics and Engineering, 2019. 17(5): 445–452.

Mahayama, M., Das, S. K., Reddy, K. R., Jain, S. Interaction of biopolymer with dispersive geomaterial and its characterization: An eco-friendly approach for erosion control. Journal of Cleaner Production, 2021. Volume: 312. https://doi.org/10.1016/j.jclepro.2021.127778

Meeuwig, R. O. Infiltration and water repellency in granitic soils. Research Paper INT-111, illus. Intermountain Forest and Range Experiment Station, Forest Serv., US Dep. Agric.: Ogden, UT, 1971. Volume: 20.

Moghal, A. A. B., Vydehi, K. V. State-of-the-art review on efficacy of xanthan gum and guar gum inclusion on the engineering behavior of soils. Innovative Infrastructure Solutions, 2021. 6: 2. DOI: 10.1007/s41062-021-00462-8

Movasat, M. and Tomac, I. (2020a). Evaluation and remediation of post-wildfire slope stability. E3S Web of Conferences, Vol. 205, EDP Sciences, 04007. DOI: 10.1051/e3sconf/202020504007.

Movasat, M. and Tomac, I. (2020b). Post-fire mudflow prevention by biopolymer treatment of water repellent slopes. Geo-Congress 2020: Biogetechnics, February 25–28, 2020 | Minneapolis, Minnesota, ASCE, GSP 320, 170-178.

Movasat, M. and Tomac, I. (2020c). Assessment of Physical Properties of Water-Repellent Soils. Journal of Geotechnical and Geoenvironmental Engineering, 147(9): 06021010.

Movasat, M. and Tomac, I. (2022a). "The Effect of Grain Size on Rainfall-Triggered Debris Flow in Hydrophobic Granular Slopes." Geo-Congress 2022, March 20–23, 2022, Charlotte, North Carolina, ASCE, GSP. 335: 417-424.

Movasat, M. and Tomac, I. (2022b). "Evaluation of Post-Impact Behavior of Single Droplet on the Hydrophobic Soil Surface." Geo-Congress 2022, March 20–23, 2022, Charlotte, North Carolina, ASCE, GSP. 335: 425-432.

NOAA (2011). National Weather Service Glossary: Closed Low, <https://forecast.weather.gov/glossary.php?word=closed+low>.

Oakley, N. S., Redmond, K. T. A Climatology of 500-hPa Closed Lows in the Northeastern Pacific Ocean, 1948–2011. Journal of Applied Meteorology and Climatology, 2014. 53(6): 1578–1592. DOI: 10.1175/JAMC-D-13-0223.1.

Oakley, N.S., Lancaster, J.T., Kaplan, M.L. Synoptic conditions associated with cool season post-fire debris flows in the Transverse Ranges of southern California. Nat Hazards, 2017. 88: 327–354. https://doi.org/10.1007/s11069-017-2867-6

Ralph, F. M., Prather, K. A., Cayan, D., Spackman, J. R., DeMott, P., Dettinger, M., Fairall, C., Leung, R., Rosenfeld, D., Rutledge, S., Waliser, D., White, A. B., Cordeira, J., Martin, A., Helly, J., Intrieri, J. CalWater Field Studies Designed to Quantify the Roles of Atmospheric Rivers and Aerosols in Modulating U.S. West Coast Precipitation in a Changing Climate. Bulletin of the American Meteorological Society, 2016. 97(7) 1209-1228. https://doi.org/10.1175/BAMS-D-14-00043.1

Savage, S. M. Mechanism of fire-induced water repellency in soil. Soil Science Society of America, 1974. Proceedings 38: 652 – 657.

Scott, D.F., van Wyk, D. B. The effects of wildfire on soil wettability and hydrological behavior of an afforested catchment. Journal of Hydrology, 1990. 121: 239 – 256.

Soldo, A., Miletić, M., Auad, M. L. Biopolymers as a sustainable solution for the enhancement of soil mechanical properties. Sci Rep, 2020. 10: 267. https://doi.org/10.1038/s41598-019-57135-x

Tiwari, B., Ajmera, B., Gonzalez, A., Sonbol, H. Impact of Wildfire on Triggering Mudslides—A Case Study of 2018 Montecito Debris Flows. Geo-Congress 2020: Engineering, Monitoring, and Management of Geotechnical Infrastructure, ASCE, Reston, VA, 40–49.

Tran, A. T. P., Chang, I., Cho G.-C. Soil water retention and vegetation survivability improvement using microbial biopolymers in drylands. Geomechanics and Engineering, 2019. 17(50): 475–483.